HIGH PRESSURE CATALYTIC REACTIONS OVER SINGLE-CRYSTAL METAL SURFACES

TEXAS A AND M UNIV., COLLEGE STATION.
DEPT. OF CHEMISTRY

1991
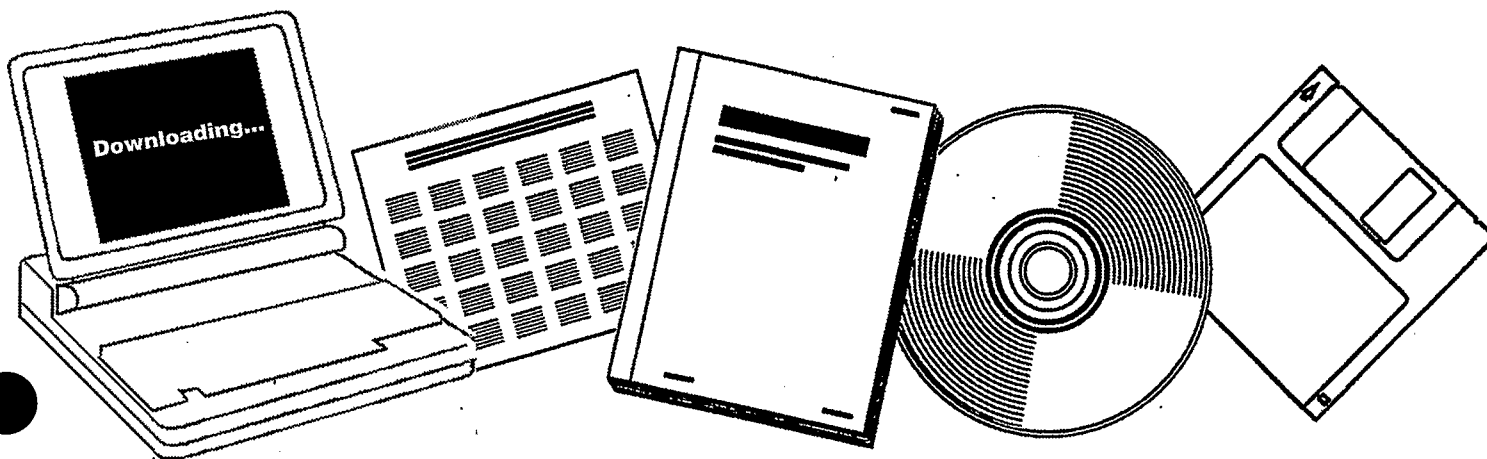
High Pressure Catalytic Reactions

Over Single-Crystal Metal Surfaces

By José A. Rodriguez and D. Wayne Goodman

Department of Chemistry
Texas A&M University
College Station, TX 77843-33255

MASTER

High-Pressure Catalytic Reactions
Over Single-Crystal Metal Surfaces

José A. Rodriguez and D. Wayne Goodman
Department of Chemistry
Texas A&M University
College Station, TX 77843-3255

CONTENTS

<u>ABSTRACT</u>

Studies dealing with high-pressure catalytic reactions over single-crystal surfaces are reviewed. The coupling of an apparatus for the measurement of reaction kinetics at elevated pressures with an ultrahigh vacuum system for surface analysis allows detailed study of structure sensitivity, the effects of promoters and inhibitors on catalytic activity, and, in certain cases, identification of reaction intermediates by post-reaction surface analysis. Examples are provided which demonstrate the relevance of single crystal studies for modeling the behavior of high surface area supported catalysts. Studies of CO methanation and CO oxidation over single crystal surfaces provide convincing evidence that these reactions are structure insensitive. For structure-sensitive reactions (ammonia synthesis, alkane hydrogenolysis, alkane isomerization, water-gas shift reaction, etc.) model single crystal studies allow correlations to be drawn between surface structure and catalytic activity. The effects of both electronegative (S and P) and electropositive (alkali metals) impurities upon the catalytic activity of metal single crystals for ammonia synthesis, CO methanation, alkane hydrogenolysis, ethylene epoxidation and water-gas shift are discussed. The roles of "ensemble" and "ligand" effects in bimetallic catalysts are examined in light of data obtained using surfaces prepared by vapor-depositing one metal onto a crystal face of a dissimilar metal.

6

I. INTRODUCTION

One of the important challenges in basic and applied science is to understand how the atomic structure, composition and electronic properties of the surface of a catalyst determine catalytic activity and selectivity. Over the past 20 years many electron spectroscopies have been developed that permit the study, on the molecular level, of surfaces and adsorbates in ultrahigh vacuum (UHV) conditions [1,2]. This has furthered our understanding of a broad range of phenomena that occur on metal surfaces: adsorbate bonding, coverage effects, coadsorption effects and reactions [1-3]. Unfortunately, the conditions under which the analytical techniques of surface science can be applied are highly idealized. The very low pressures required for surface science studies are typically many orders of magnitude below the pressures used in practical catalytic processes. In order to overcome this problem, several laboratories have developed experimental systems which combine a high pressure reactor system with an UHV analysis chamber [4-9]. The high pressure reactor allows the kinetics of catalytic reactions to be measured on a given surface, while analysis of the structure and composition of the surface both before and after reaction can be accomplished in the UHV analysis chamber. In many high-pressure/UHV studies a clean and well-defined, single-crystal plane is used to model a site or set of sites expected to exist on practical high-surface-area catalysts. This approach allows direct comparison of reaction rates measured on single crystal

surfaces with those measured on more realistic supported metal catalysts, and also allows detailed study of structure sensitivity, the effects of promoters and inhibitors on catalytic activity, and, in certain cases, identification of reaction intermediates by post-reaction surface analysis.

In this article, we review existing literature that deals with high-pressure catalytic reactions on metal single-crystal surfaces. We focus our attention in the kinetics and surface chemistry of the catalytic reactions. Examples are provided which demonstrate the relevance of single crystal studies for modeling the behavior of high surface area supported catalysts. For an excellent review on the instrumentation used in this type of experiments we refer the reader to ref. [9].

II. AMMONIA SYNTHESIS

The success of ammonia synthesis ($N_2 + 3H_2 \rightarrow 2NH_3$) as a method of nitrogen fixation was a landmark in the development of catalytic processes [10,11]. The search for a catalyst was conducted by Haber, Bosh and Mittasch in the laboratories of Badische Arilin und Soda Fabrik (BASF) between about 1905 and 1910. The discovered catalyst contained iron with some alumina and potassium oxide. Large-scale production of synthetic ammonia using such a catalyst started in Germany in 1914. The industrial catalysts used today are based mainly on iron promoted with Al_2O_3, K_2O, CaO and MgO [10]. Although the kinetics of the ammonia synthesis reaction has been investigated by numerous

8

workers, the mechanism of the reaction is by no means unequivocally established.

II.1 Kinetics over Fe single-crystal catalysts.

The adsorption and dissociation of N_2, H_2 and NH_3 on the (100), (110) and (111) faces of iron have been investigated in detail under UHV conditions. The initial sticking coefficient for dissociative nitrogen chemisorption was found to be very low (10^{-7}–10^{-6}), with the activity of the surfaces following the sequence: (111) > (100) > (110) [12,13]. On Fe(100), atomic N forms a c(2x2) structure [12]. By contrast, the Fe(111) and Fe(110) planes reconstruct under the influence of N atoms. A series of complicated LEED patterns was observed in these cases, which could be reconciled with slightly distorted (111) planes of Fe_4N on top of the iron substrate [12,13]. The activation energy for nitrogen desorption ranges between 210 and 240 kJmol^{-1} (depending on the surface orientation). From this the strength of the Fe-N bond is estimated to be ~580 kJmol^{-1} [12,13], which can be compared with the value of 950 kJmol^{-1} reported for the dissociation energy of N_2.

The dissociative adsorption of H_2 on the (100), (110) and (111) faces of iron is non-activated and proceeds with initial sticking coefficients in the range between 0.1 and 0.2 [14,15]. At the limit of zero coverage, the strength of the Fe-H bond is of the order of ~250 kJmol^{-1} [14,15]. The initial hydrogen adsorption energy varies between 88 and 110 kJmol^{-1} on the

various crystal planes [14,15]. At low temperatures (<200K) NH_3 adsorbs non-dissociatively on the Fe(100), Fe(110) and Fe(111) surfaces [16,17]. The heat of adsorption depends on substrate orientation and adsorbate coverage showing a maximum value of 70 $kJmol^{-1}$. Over Fe, NH_3 decomposition occurs stepwise yielding $NH_{2,a}$, NH_a and H_a [16,17].

On the basis of information obtained by using single-crystals under UHV conditions, the individual reaction steps for ammonia synthesis can be formulated as follows [18]:

$$H_{2,g} = 2H_a \tag{1}$$

$$N_{2,g} = N_{2,a} = 2N_a \tag{2}$$

$$N_a + H_a = NH_a \tag{3}$$

$$NH_a + H_a = NH_{2,a} \tag{4}$$

$$NH_{2,a} + H_a = NH_{3,a} \tag{5}$$

$$NH_{3,a} = NH_{3,g} \tag{6}$$
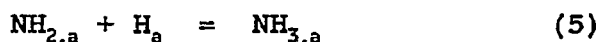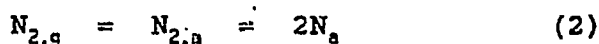
In this mechanism the rate-limiting step is the dissociation of adsorbed N_2 [18,19]. A kinetic model constructed using this mechanism and parameters derived from quantum – mechanical calculations and from the UHV studies described above predicts rates of NH_3 synthesis that are in excellent agreement with high-pressure measurements over industrial catalysts [19].

At 798K and a total pressure of 20 atm of a stoichiometric mixture of hydrogen and nitrogen ($P_{H2}/P_{N2} = 3$), ammonia was formed on Fe(111) at a rate of 4.6×10^{-8} moles $cm^{-2}s^{-1}$ with an activation energy of 81.2 $kJmol^{-1}$ [20]. The activity ratio of Fe(111):Fe(100):Fe(110) for NH_3 synthesis was found to be

418:25:1 [20]. The same order of reactivity has been found for the dissociative chemisorption of N_2 (see above), the rate-determining step in the ammonia synthesis reaction.

The high catalytic activity of Fe(111) can be attributed to the presence of metal atoms with a coordination number of 7 (C_7 coordination sites: the most highly coordinated surface sites Fe can expose), which are in the second and third layers and are exposed to the reactant gases [21]. A second possibility is that since the Fe(111) surface is very open, the high catalytic activity is due to the high surface free energy and low work function that are characteristic of a rough surface [21]. The high pressure kinetic data presented in Fig. 1 for ammonia synthesis over Fe(111), Fe(211), Fe(100), Fe(210) and Fe(110) show that the presence of highly coordinated sites is more important than surface roughness for catalytic activity [21]. The Fe(210) plane contains no C_7 sites but it is an open face exposing second and third layer atoms, much like the Fe(111) plane. On the other hand, the Fe(211) crystal contains C_7 sites but it is less open than the Fe(210) face. If surface roughness was the important ingredient for an active iron catalyst then one would expect Fe(210) to be the most active surface in Fig. 1. The results are contrary to this expectation, showing that the Fe(211) crystal is almost as active as Fe(111), while the Fe(210) is much less active. The experimental data support the contention that C_7 sites are the most active centers in iron ammonia synthesis catalysts [21].

11

The surfaces of industrial catalysts are promoted with K_2O [10]. Model studies with adsorbed potassium (without oxygen) on Fe(100) indicate that small K concentrations increase the sticking coefficient for dissociative N_2 adsorption (the rate-limiting step in NH_3 synthesis) by more than two orders of magnitude up to a maximum value of 4×10^{-5} (at 430K) [18]. N_2 is more tightly held in the vicinity of an adsorbed K atom. The N_2 adsorption energy is in fact increased from 30 $kJmol^{-1}$ to 45 $kJmol^{-1}$, while simultaneously the activation energy for dissociation is lowered by ~10 $kJmol^{-1}$ [18]. Adsorption of K on Fe surfaces causes a very pronounced lowering of the work function; this enhances back-donation of metallic electrons to the antibonding $N_2(2\pi)$ orbital, strengthening the $M-N_2$ bond and weakening the N-N bond.

Over actual ammonia synthesis catalysts the promoter effects of K are reduced by coadsorbed oxygen [18]. Under reaction conditions K alone is not thermally stable on Fe surfaces. Addition of oxygen or aluminum oxide prevents the desorption of K, keeping a relatively large concentration of this promoter on the surface of the catalyst [18,20b]. Studies of ammonia synthesis (T= 673-723K with a 20-atm stoichiometric mixture of N_2 and H_2) over iron surfaces doped with K and K+O [20] show no promotional effect on Fe(110) and a marked increase in the reaction rate on Fe(111) and Fe(100). No change in the apparent activation energy of the reaction was observed when K was added to the Fe surfaces [20c]. To explain these results, a kinetic

model has been proposed in which potassium enhances the rate of ammonia synthesis by lowering the concentration of NH_3 on the surface (making more active sites available to chemisorb the reactants) and by increasing the rate of N_2 dissociation [20c].

II.2 Kinetics over Re single-crystal catalysts.

The synthesis of ammonia from N_2 and H_2 was investigated over model single-crystal rhenium catalysts at 20 atm reactant pressure ($P_{H2}/P_{N2} = 3$) and temperatures between 720 and 900K [22]. The results of Fig. 2 indicate that ammonia synthesis is a structure sensitive reaction over Re surfaces. An apparent activation energy of 81.2 ± 4.6 kJmol^{-1} was observed, regardless of the catalyst surface structure [22]. Kinetic data, reactant pressure dependence and deuterium isotope effect indicate that the rate-determining step is the dissociative chemisorption of N_2, as in the case of Fe catalysts [22].

In Fig. 2 the most active crystal faces are those that expose highly coordinated C_{11} and C_{10} sites [21]. Surface roughness on the Re catalyst is only important to the extent that it can expose these highly coordinated surface atoms. An identical result was obtained for Fe substrates (see above). Theoretical work suggest that highly coordinated metal atoms will show the greatest catalytic activity because these atoms can experience the largest electronic charge fluctuations within the solid [21]. On these highly coordinated sites bond breaking and

13

bond formation can occur within the lifetime of the reaction intermediates.

III. CO METHANATION

The reaction of low concentrations of CO in a mixture with H_2 to form CH_4 was developed as a gas-purification process in the 1950s [10]. At the present time, the methanation reaction has a critical role in the production of synthetic natural gas from hydrogen-deficient carbonaceous materials [10,23,24]. In addition, the reaction is an obvious starting point in studies of fuel and chemical synthesis from carbon sources [10,23,24]. In the last ten years the methanation reaction over single crystal surfaces has been the subject of many investigations. Here we review the results of these investigations. We begin with a discussion of the studies on monometallic (section III.1.1) and bimetallic (section III.1.2) single crystal surfaces. Next the results of studies dealing with the effects of electronegative (section III.2.1) and electropositive (section III.2.2) impurities on the kinetics of the methanation reaction are presented. Finally, we show studies concerned with metal-support interactions and the methanation reaction (section III.3).

III.1 CO Methanation on clean metal single crystals.

III.1.1 Monometallic surfaces

A. Ni(100) and Ni(111)

The data in the Arrhenius plot of fig. 3a represent steady-state specific methanation rates (CH_4 molecules/site-s) on both the Ni(111) and Ni(100) surfaces [25]. At a given temperature the rate of production of CH_4 over an initially clean catalyst crystal was constant, with no apparent induction period [25]. The atomic configurations of the Ni(100) and Ni(111) surfaces are shown in figs. 3b and 3c, respectively. The similarity between the data for the close-packed (111) and for the more open (100) crystal plane of Ni is evident in both the specific rates and activation energy (103kJ/mol). The single crystal results are compared in fig. 3a with three sets of data taken from ref. [26] for alumina supported nickel catalysts. This comparison shows extraordinary similarities in kinetic data taken under nearly identical conditions. Thus, for the H_2 + CO reaction over nickel, there is no significant variation in the specific reaction rates or the activation energy as the catalysts change from small metal particles to bulk single crystals. These data provide convincing evidence that the methanation reaction rate is indeed structure insensitive on nickel catalysts.

Post-reaction analysis of the surface of the Ni crystal catalysts with Auger electron spectroscopy (AES) showed a low level of a carbon species and the absence of oxygen [6,25]. The Auger lineshape for the carbonaceous residue was similar to that

15

of nickel carbide, indicating that the carbon was in a "carbidic" form [6]. Experiments were carried out studying the interaction of CO (24 Torr, 0-1000s exposures) with Ni(100) at different temperatures (450-800K) [27]. AES data showed the deposition of carbon on the surface and the absence of oxygen. Two kinds of carbon were formed on the surface: a carbidic type which occurs at temperatures <650K and a graphite type at temperatures >650K. The carbidic type saturates at 0.5 monolayers, and can be readily removed from the Ni(100) surface by heating the crystal to 600K in 1 atm of H_2 with methane formed as the product. In contrast, the graphitic type is a poison. The deposition of an active carbon residue and the absence of oxygen on the nickel surface following heating in pure CO is consistent with a well-known disproportionation reaction, the Boudouard reaction,

$$2CO_g \rightarrow C_a + CO_{2,g} \qquad (7)$$

which has been studied on supported Ni catalysts [28,29] and on Ni films [30]. On Ni(100), the carbon formation data from CO disproportionation indicates a rate equivalent to that observed for methane formation in a H_2/CO mixture. Therefore, the surface carbon route to product is sufficiently rapid to account for methane production with the assumption that kinetic limitations are not imposed by the hydrogenation of this surface carbon.

A set of experiments was performed [27] in which a Ni(100) surface was precarbided by exposure to CO and then treated with hydrogen in the reaction chamber for various times. This study showed that the rate of carbon removal in hydrogen compared

favorably to the carbide formation rate from CO and to the overall methanation rate in H_2/CO mixtures. Thus in a $H_2 + CO$ atmosphere the methanation rate is determined by a delicate balance of the carbon formation and removal steps and neither of these is rate determining in the usual sense [6,25,27]. More recent studies [31] using isotopically labeled CO have shown that the CO dissociation step is essentially unidirectional in that the rate of C_a and O_a recombination is insignificantly slow compared to the C_a hydrogenation rate.

Figure 4a shows the changes in the methanation reaction rate as the total pressure is increased from 1-120 Torr at a fixed $H_2:CO$ ratio [25]. At low temperatures the rates fall on the same straight line at all pressures. As the temperatures is increased, a deviation from linearity is seen – the higher the pressure the higher the deviation temperature. Accompanying this non-linear rate behavior is an increase in the active carbon level on the surface of the catalyst crystal [25]. It has been proposed [25] that this departure from the linearity of the rate in fig. 4a and the accompanying increase in the surface carbon level is due to a decrease in the surface coverage of hydrogen and thus a decrease in the rate of hydrogenation of surface carbon. According to the mechanism proposed above for CO methanation, if reaction conditions are altered such that the surface hydrogen concentration decreases (e.g. low H_2 pressure and high temperature) then a correlation between decreasing methane yield and increasing surface carbide should be observed.

17

This correlation holds very well as evidenced by the data in fig. 5. Thus, the proposed reaction mechanism involving the dissociation of CO and the subsequent hydrogenation of the resulting carbon species (C_a) accounts quite satisfactorily for the effect of pressure on the methanation rate, for the variation in the measured surface carbon level as reaction parameters are changed, and for the formation at characteristic temperature and pressure conditions of a catalyst-deactivating graphitic carbon.

B. Ru(110) and Ru(001)

Figure 4b displays steady state specific rates for CO methanation on two faces of ruthenium: the zig-zag, open (110), and the close-packed (001) [25]. While the comparison is limited, it is clear that the H_2 + CO reaction is quite similar in regard to the specific reaction rate and the activation energy for these two crystal planes of ruthenium. Thus, it appears that CO methanation is structure insensitive on ruthenium surfaces [25].

Post-reaction surface analysis of the Ru crystal catalysts with AES showed the presence of carbidic carbon [25]. The hydrogenation of this carbonaceous residue can be followed readily [25,32]. Furthermore, the specific rates of carbide formation on ruthenium surfaces from CO decomposition are equal to the rates of methane formation in CO + H_2 mixtures [25,32]. This experimental evidence suggests that the reaction mechanism for CO methanation on ruthenium surfaces is similar to that

18

mentioned above for methanation over nickel surfaces. In fig. 4 the variation of the reaction rate with pressure is very similar for the Ni(100) and Ru(110) crystals. In both cases, the non-linear rate behavior is accompanied by an increase in the active carbon level on the surface of the catalyst crystal. It has been proposed [25] that the departure from linearity of the rate in fig. 4 is due to a decrease in the surface coverage of hydrogen, which causes a decrease in the rate of hydrogenation of surface carbon. In fact, since the binding energy of hydrogen on Ru is lower than on Ni [25,33], the deviation from linearity should be expected at lower temperature for ruthenium. This is particularly evident in the 1 Torr data of figs. 4a and 4b.

C. W(110)

The methanation activities for W(110) [34] and Ni(100) [24] are compared in fig. 6 over a range of temperatures (fig. 6a) and H_2 partial pressures (fig. 6b). The data clearly indicate that W(110) is an active methanation catalyst, with an activity that in some cases can surpass the activity of Ni(100). Plotting the data in an Arrhenius fashion (fig. 6a) yields an apparent activation energy of 56 kJmol^{-1} for W(110), as compared to 103 kJmol^{-1} for Ni(100). The activation energy over W(110) is in reasonable agreement with the value of 63 kJmol^{-1} observed on catalysts prepared by decomposition of $W(CO)_6$ on alumina [35].

Auger electron spectra of the W(110) surface after steady-state reaction conditions indicated that the active methanation

19

surface was highly carbidic [34], in contrast to the case of nickel, where the active methanation surface is the metal itself with only a low surface coverage (0.05-0.1 monolayers) of carbidic carbon species present [6,25]. The idea that the active W surface is carbidic is consistent with the significant hydrogenation activity reported for W carbide catalysts [34].

D. Rh(111)

CO hydrogenation over clean Rh(111) was studied at a temperature of 573K and partial pressures of 4.5 atm of H_2 and 1.5 atm of CO [36]. Under these reaction conditions the Rh catalyst produced primarily methane (90 wt%) at an initial rate of 0.15 molecules/site-s. Small amounts of C_2 and C_3 hydrocarbons were also formed, but no oxygenated hydrocarbons were detected. The rates of formation of all the products were found to be the same on the Rh(111) single crystal and on a pollycrystalline Rh foil suggesting that CO hydrogenation is structure insensitive on these surface [36]. The results of AES showed the presence of ~1 monolayer of carbon on the surface of the Rh catalysts after 3 hours of reaction [36]. The close proximity of the Rh 256 and 302 AES peaks to the C 272 AES peak prevented an analysis of the lineshape of the carbon peak in order to determine the chemical nature of the carbonaceous residue.

E. Fe(111)

The hydrogenation of CO on the (111) face of iron was examined at partial pressures of 4.5 atm of H_2 and 1.5 atm of CO and at a temperature of 573K [37]. The major product of the reaction was methane (~70 wt%), which was formed at an initial rate of 1.35 molecules/site-s. The formation of C_2 (~20 wt%), C_3 and C_4 products was also observed.

F. Mo(100)

Figure 7 shows the effects of temperature and pressure on the rate of CO methanation over Mo(100). On this surface, the hydrogenation of CO produced primarily methane (~90 mol%), ethene and propene [38]. An activation energy of ~100 kJ/mole was found for the methanation reaction on Mo(100). The observed rate law for methanation (see fig 7b) is given by:

$$r_{CH4} = kP_{CO}^{+0.32} P_{H2}^{+1.0} \tag{8}$$

The positive power of rate dependence on the pressure of CO is unusual since the methanation rate has a negative-order dependence on CO partial pressure over Ni, Ru, Fe and Co catalysts [5,38,39].

Auger electron spectra taken after the hydrogenation reaction indicate that the "active" surface is covered by a submonolayer of a carbidic carbon species. The reaction is poisoned as the carbidic species is converted to graphitic carbon. The rate of poisoning is determined by the ratio of CO to H_2 in the reaction mixture and by the reaction temperature

(lower $CO:H_2$ ratios and lower temperatures prolong the lifetime of the active catalyst).

The following set of elementary steps was proposed for the methanation reaction on Mo(100) [38]:

$$CO_g \rightleftharpoons CO_a \qquad\qquad (9)$$

$$H_{2,g} = H_{2,a} \qquad\qquad (10)$$

$$CO_a + H_{2,a} = CHOH_a \qquad\qquad (11)$$

$$CHOH_a + 1/2\ H_{2,a} \rightarrow CH_a + H_2O \qquad\qquad (12)$$

$$CH_a + 3/2\ H_{2,a} \xrightarrow{\text{fast}} CH_{4,g} \qquad\qquad (13)$$
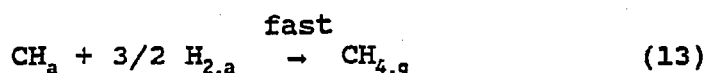
In terms of this model the rate-determining step is reaction (12) and all the steps preceding it are in quasiequilibrium. A mathematical analysis of this kinetic model [38] leads to a rate expression of the form:

$$r_{CH4} = kP_{CO}^{+0.5}P_{H2}^{+1.0}, \qquad\qquad (14)$$

which is in reasonable agreement with the experimental results of fig. 7b. Reactions (9) to (13) probably take place on top of a carbidic overlayer [38]. This overlayer will deactivate by forming graphite on the surface, which will block the reaction sites.

No differences in either rates or product distributions were observed between CO hydrogenation on Mo(100) and over pollycrystalline Mo foils [38]. Thus, the reaction does not appear to be structure sensitive on molybdenum surfaces.

G. Co(0001), Co(11$\bar{2}$0) and Co(10$\bar{1}$2)

CO hydrogenation over Co(001) was investigated at temperatures between 490 and 570K, and partial pressures of 0.66 atm of H_2 and 0.33 atm of CO [40]. Under this reaction conditions methane was the major product, with lesser amounts of heavier hydrocarbons. The apparent activation energies for methane, ethane and propane formation were found to be equal (~70 kJ/mol, T<570K), which suggests a similar rate-determining step [40]. The HREELS spectrum, taken after the reaction, showed peaks at 2980, 1420 and 845 cm^{-1}, which can be attributed to vibrations of adsorbed CH_x(x = 1,2,3) groups [40].

Studies for CO hydrogenation on Co(0001), Co(11$\bar{2}$0) and Co(10$\bar{1}$2) show very similar rates of methane production over these surfaces [40]. The apparent activation energy for CO methanation is identical on Co(0001) and Co(11$\bar{2}$0) (70 kJ/mol) [40]. However, the product distribution for heavy hydrocarbons (MW > 16) is different. Co(11$\bar{2}$0) yielded a larger chain growth probability than Co(0001). Post-reaction spectroscopy with HREELS and AES revealed that during the reaction longer chain hydrocarbon fragments grew on Co(11$\bar{2}$0), while on Co(0001) only CH_x (x = 1-3) species were observed [40].

H. Summary

Table I shows the apparent activation energies observed for CO methanation on different single crystal surfaces. In general, the energies are close to the value of 110 kJ/mol. The

exceptions are W(110) and Co(001), with apparent activation energies of 56 and 70 kJ/mol, respectively. The studies reviewed in this section provide convincing evidence that the methanation reaction is structure insensitive on surfaces of Ni, Ru, Rh, Fe and Mo. On these metals the methanation of CO occurs in the presence of an active carbidic overlayer. The transformation of this overlayer into graphite leads to a decrease in the catalytic activity of the metal surfaces.

III.1.2 Bimetallic surfaces

Catalytic properties of metal surfaces can be altered greatly by the addition of a second transition metal [41]. In many cases, mixed-metal systems are superior over their single-metal counterparts in terms of catalytic activity and/or selectivity [41]. Many fundamental studies have focussed on trying to understand the roles of "ensemble" and "ligand" effects in bimetallic catalysts [41,42]. Ensemble effects are defined in terms of the number of surface atoms needed for a catalytic process to occur. Ligand effects refer to those modifications in catalytic activity or selectivity that are the product of electronic interactions between the components of a bimetallic system. In gathering information to address these issues, it has been advantageous to simplify the problem by utilizing models of bimetallic catalysts such as the deposition of metals onto single-crystal substrates. Work on ultrathin metal films supported on well-defined metal surfaces (Cu on Ru(001) [43-46];

Cu, Ni, Pd and Pt on W(110) and W(100) [47-51]; Fe, Ni and Cu on Mo(110) [52,53]; and Fe and Cu on Re(001) [53,54]) has shown that a metal atom in a matrix of a dissimilar metal can be significantly perturbed, and that this perturbation can dramatically alter the chemical and electronic properties of both constituents of the mixed-metal system.

The studies reviewed here are part of a continuing effort to identify those electronic and structural properties of bimetallic systems which can be related to their superior catalytic abilities.

A. Ni/W(110) and Ni/W(100)

The Ni/W(100) and Ni/W(110) systems are particularly interesting because they involve the addition of an active metal for CO methanation (Ni) to relatively inactive tungsten surfaces.

At ~100K, Ni is adsorbed layer by layer on W(110) and W(100) [49]. The results of low-energy electron diffraction (LEED) indicate that at coverages up to 1 ML the Ni films grow pseudomorphically with respect to the W(110) and W(100) substrates [49]. This growth pattern leads to Ni monolayer densities on W(110) and W(100) which are 21% and 38% less than the corresponding monolayer densities for Ni(111) and Ni(100), respectively.

Specific rates of CH_4 production, expressed as turnover frequencies (CH_4 molecules/Ni atom-s), over Ni covered W(110) and W(100) surfaces are shown in fig. 8 [51]. Under the experimental

conditions of this figure, the reaction rates on the clean W surfaces were ~10^2 times lower than on the Ni covered surfaces. Figure 8a shows that for a total pressure of 120 Torr, Arrhenius behavior is observed over the entire temperature range studied (450-700K) as the CH_4 production rates vary by almost 3 orders of magnitude. The similarity between Ni/W(110) and Ni/W(100) at all the coverages studied is evident in both the turnover frequencies and activation energy, 77 ± 4 kJ/mole. The activation energy for the Ni covered W surfaces is lower than the value of 103 kJ/mole reported for Ni(100) and Ni(111) [25]. However, the specific rates for CO methanation on Ni/W(110) and Ni/W(100) correlate well with those observed on supported Ni catalysts, Ni single crystals and Ni films [51]. These results are further manifestations of the structure insensitive behavior of the CO methanation reaction and suggest that the mechanistic steps which control the rate of CO hydrogenation are the same in all these surfaces.

Lowering the total pressure has a significant effect on the rate of methane production (Figure 8b) for Ni supported on W(110) [51]. A similar effect was observed for Ni(100) (see figure 4a), and was attributed to a decrease in the concentration of atomic hydrogen on the surface as the pressure was lowered and the temperature was increased (see section III.1.1) [25]. The departure from Arrhenius behavior occurs at lower temperature for Ni/W(110). This correlates [51] with the fact that the

activation energy for H_2 desorption from Ni/W(110) (~71 kJ/mol [49]) is lower than that from Ni(100) (96 kJ/mol [55]).

B. Cu/Ru(001) and Ag/Rh(111)

A bimetallic system that has been extensively studied in supported catalyst research is copper on ruthenium [41,45,46]. The immiscibility of copper in ruthenium circumvents the complication of determining the three dimensional composition. The adsorption and growth of copper films on the Ru(0001) surface have been examined [43,44,56,57] by work function measurements, LEED, AES, XPS and TPD. The experimental evidence indicates that for submonolayer depositions at 100K the Cu grows in a highly dispersed mode, forming 2-D islands pseudomorphic to the Ru(001) substrate upon annealing to 300K. The pseudomorphic growth implies that the copper-copper bond distances are strained approximately 6% beyond the equilibrium bond distances found for bulk copper.

Copper surfaces are inactive catalysts for CO methanation. A study of the rate of CO methanation over Cu/Ru(001) [46] indicates that copper merely serves as an inactive diluent, blocking the active sites of the ruthenium surface in a one-to-one basis. Similar results have been found in analogous studies [58] introducing silver onto a Rh(111) methanation catalyst.

C. Co/W(110) and Co/W(100)

Cobalt forms pseudomorphic monolayers on W(110) and W(100) which are thermally stable to 1300K [59]. The cobalt overlayers are geometrically strained with respect to bulk cobalt surfaces. The pseudomorphic monolayer of Co/W(110) has an atomic density 21% less than Co(001), while the pseudomorphic monolayer of Co/W(100) has an atomic density 45% less than Co(001) [59]. However, the CO methanation activity of these Co/W surfaces is very similar and compares favorably with that of alumina supported Co catalysts [59]. A fact that suggests that CO methanation is structure insensitive on cobalt surfaces [59].

AES spectra showed the after-reaction Co/W surfaces to have high coverages of both carbon and oxygen, with carbon lineshapes characteristic of carbidic carbon [59]. The catalytic activity is apparently not correlated with surface carbon level [59].

III.2 CO Methanation in chemically modified surfaces.

The addition of impurities to a metal catalyst can produce dramatic changes in the activity, selectivity and resistance to poisoning of the catalyst. For example, the selectivity of some transition metals can be altered greatly by the addition of light metals such as potassium, and the activity can be reduced substantially by the addition of electronegative species such as sulfur. Although these effects are well-recognized in the catalytic industry, the mechanisms responsible for chemical changes induced by surface additives are poorly understood. An

important question concerns the underlying relative importance of ensemble (steric or local) versus electronic (nonlocal or extended) effects. A general answer to this question will improve our ability to design efficient catalysts.

Catalyst deactivation and promotion are extremely difficult questions to address experimentally [60]. For example, the interpretation of related data on high-surface area supported catalysts is severely limited by the uncertainty concerning the structural characterization of the active surface. Specific surface areas cannot always be determined with adequate precision. In addition, a knowledge of the crystallographic orientation, the concentration and the distribution of impurity atoms, as well as their electronic states is generally poor. The use of metal single crystals in catalytic reaction studies essentially eliminates the difficulties mentioned above and allows, to a large extent, the utilization of a homogeneous surface amenable to study using modern surface analytical techniques. In this section we review studies dealing with the effects of electronegative and electropositive surface impurities on the rates of CO methanation over single crystal catalysts. Although the studies to date are few, the results appear quite promising in addressing fundamental aspects of catalytic poisoning and promotion.

III.2.1 Electronegative impurities

Impurities whose electronegativities are greater than those for transition metals generally poison a variety of catalytic reactions, particularly those involving H_2 and CO. Of these poisons sulfur is the best known and is technologically the most important [10,60].

A. Atomic chlorine, sulfur and phosphorus on Ni(100)

The effects of preadsorbed Cl, S and P atoms on the adsorption-desorption of H_2 and CO on Ni(100) have been extensively studied [61-65] using Auger electron spectroscopy, low-energy electron diffraction and temperature programmed desorption. Figure 9 shows the variation of the saturation coverage of H and CO on Ni(100) with the coverage of Cl, S and P. Both CO and H_2 adsorption decrease markedly in the presence of surface impurities. The effects of P, however, are much less pronounced than for Cl and S. The similarity in the atomic radii of Cl, S and P (0.99, 1.04 and 1.10Å, respectively [66]) suggests a relationship between electronegativity and the poisoning of chemisorptive properties by these surfaces impurities [61-63]. Impurities that are strongly electronegative with respect to nickel, Cl and S, modify the chemisorptive behavior far more strongly than would result from a simple site blocking model. The initial effects of these impurities as shown in Fig. 9 indicate that a single impurity atom can successfully poison more than just its nearest-neighbor nickel atoms. This type of

poisoning supports an interaction that is primarily electronic in nature.

The experimental results [61-63] indicate that the presence of electronegative Cl, S and P atoms causes a reduction of the adsorption rate, the adsorption bond strength and the capacity of the Ni(100) surface for CO and H_2 adsorption. In general, these poisoning effects become stronger with increasing electronegativity of the adsorbed impurity.

Kinetic studies [61-63] have been carried out for CO methanation over Ni(100) surfaces covered with chlorine, sulfur and phosphorus impurities. Figure 10 shows the rate of CO methanation as a function of sulfur and phosphorus coverage over a Ni(100) catalyst at 120 Torr and a H_2/CO pressure ratio equal to 4. In the case of Cl overlayers no change in the methanation rate was observed. At the reaction conditions of fig. 10, H_2 reacts with the adsorbed Cl forming HCl. This reaction "cleans" the Ni(100) surface and prohibits the study of the effects of Cl on the methanation kinetics. The results presented in fig. 8 correlate very well with the studies on the effects of S and P overlayers upon the adsorption of H_2 and CO on Ni(100) ([61-63] and fig. 9.)

Figure 10 shows a non-linear relation between the sulfur coverage and the methanation rate. A steep drop in catalytic activity is observed at low sulfur coverages, and the poisoning effect maximizes quickly. A similar reduction of methanation activity by sulfur poisoning has been observed for alumina

supported nickel catalysts [67]. The initial attenuation of catalytic activity by sulfur suggests that ten or more equivalent nickel sites are deactivated by one sulfur atom. There are two possible explanations for this result: (1) an electronic effect that extends to the next-nearest-neighbor sites or (2) an ensemble effect, the requirement being that a certain number of surface atoms is necessary for a reaction to occur. If extended electronic effects are significant, then the reaction rate is expected to be a function of the relative electronegativity of the poison. In contrast, if an ensemble of ten nickel atoms is required for the critical step of methanation, then altering the electronegative character of the poison should produce little change in the poisoning of the reaction. Substituting phosphorus for sulfur (both atoms are approximately the same size [66]) results in a marked change in the magnitude of poisoning at low coverages as shown in fig. 10. Phosphorus, because of its less electronegative character, effectively poisons only the four nearest-neighbor metal atom sites. These results support the conclusion that extended electronic effects do play a major role in catalytic deactivation by sulfur.

B. Atomic Sulfur on Ru(001), Rh(111) and W(110)

Figure 11 presents the effects of sulfur coverage on the rate of CO methanation on Ru(001) and Rh(111) catalysts [58,68]. As for the case of Ni(100), a precipitous drop in the catalytic activity is observed for low sulfur coverages. The initial

32

changes in the rates suggest that more than ten Rh or Ru atom

sites are deactivated by one sulfur atom.

Kinetic data for sulfur-covered W(110) surfaces indicate

that the activation energy of the methanation reaction does not

change with sulfur coverage [69]. In this respect tungsten is

similar to nickel [61]. Sulfur decreases the rate of CO

methanation on W(110) [69]. In fig. 12 the relative change in

rate is plotted as a function of sulfur coverage. For

comparison, the data for the Ni(100) surface [61] are included.

While sulfur clearly exhibits long-range effects on nickel, the

operation of long-range effects over tungsten occurs only at the

lowest coverages. At very low sulfur coverages (~0.03 ML), the

decrease in activity is quite steep and extrapolates to between

10 and 12 atoms sites deactivated per sulfur atom adsorbed [69].

Apparently the adsorption of sulfur occurs initially in a random,

disordered fashion, so that there is little overlap of the

inhibiting effect of sulfur atoms on open sites. As the sulfur

coverage increases, clustering into islands occurs [69]. Thus,

the inhibiting effect of additional sulfur atoms is diminished

due to overlap with the effect of previously adsorbed sulfur

atoms.

III.2.2 Electropositive impurities

We have discussed above the role of electronegative

impurities in poisoning Ni(100), Ru(001), Rh(111) and W(110)

toward methanation activity. These results have been ascribed,

33

to a large extent, to an electronic effect. In the context of this interpretation it is expected that an electropositive impurity might have the opposite effect, i.e. to increase the methanation activity of a metal surface. A study of CO hydrogenation over potassium covered Ni(100) [63,70] has shown that this is not the case, although certain steps in the reaction mechanism are strongly accelerated by the presence of the electropositive impurity.

A. Potassium on Ni(100)

Figure 13 shows kinetic measurements of CO methanation over a Ni(100) catalyst containing well-controlled submonolayer quantities of potassium adatoms [70]. These data indicate a decrease in the steady-state rate of methanation with potassium coverage. A coverage of about 0.22 ML of potassium would be sufficient to terminate the reaction completely. The presence of K did not alter the apparent activation energy associated with the kinetics, as shown in the Arrhenius plot of fig. 13b. However, the potassium did change the steady-state coverage of active carbon on the catalyst. This carbon level changed from 10% of a monolayer on the clean catalyst to 30% of a monolayer for a catalyst covered with 0.1 ML of potassium [70].

As shown in fig. 14, adsorbed potassium caused a marked increase in the steady-state rate and selectivity of Ni(100) for higher hydrocarbon (MW>16) synthesis [70]. At all the temperatures studied, the overall rate of higher hydrocarbon

34

production was faster on the potassium-dosed surfaces, so that potassium may be considered a true promoter with respect to this reaction, Fischer-Tropsch synthesis. The effects of potassium upon the kinetics of CO hydrogenation over Ni(100) (i.e. a decrease in the rate of methane formation and an increase in the rate of higher hydrocarbon production) are similar to those reported for high-surface-area supported Ni catalysts [71-72]. This agreement between bulk, single crystal Ni and supported Ni indicates that the major mechanism by which potassium additives alter the activity and selectivity of industrial catalysts is not related to the support material, but that it is rather a consequence of direct K-Ni interactions.

Adsorbed potassium causes a marked increase in the rate of CO dissociation on a Ni(100) catalyst [70]. The increase of the initial formation rate of "active" carbon or carbidic carbon via CO disproportionation is illustrated in Fig. 15. The relative rates of CO dissociation were determined for the clean and potassium covered surfaces by observing the growth in the carbon Auger signal with time in a CO reaction mixture, starting from a carbon-free surface. The rates observed in fig. 15 are the observed rates of carbon formation extrapolated to zero carbon coverage. The presence of K adatoms leads to a reduction of the activation energy of reactive carbon formation from 96 kJ/mol on clean Ni(100) to 42 kJ/mol on a 10% potassium covered surface [70].

In spite of increasing the rate of CO dissociation or carbide buildup, potassium decreases the overall rate of methanation. This reduction in methanation activity must be related to a poisoning of either the hydrogen adsorption or the hydrogen addition steps [70]. The enhancement of steady-state carbide coverage caused by potassium favors C-C bond formation and the synthesis of heavy hydrocarbons (MW>16).

III.2.3 Related theory

CO is generally thought to be adsorbed on transition-metal surfaces by the Blyholder mechanism [73,74], which involves σ-donation of electron density from CO into the unoccupied metal orbitals and π-back-donation of electron density from occupied metal orbitals into the lowest unoccupied molecular orbitals ($2\pi^*$) of the CO molecule. The mechanism is similar to that observed for CO bonding in transition metal compounds [75]. Theoretical results with the constrained space orbital variation (CSOV) method show that, in this type of synergistic bond with σ-donation/π-back-donation, π-back-donation is energetically more important in determining the character of the bond than is σ-donation, at least for the case of Cu surfaces [76-78]. Recently, inverse photoemission results have supported the predominant importance of $2\pi^*$ back-donation in CO chemisorption on Pd and Ru [79]. The thought that the antibonding 2π orbitals of CO are populated upon adsorption is consistent with the results of HREELS [80,81], which show that the C-O stretching

36

frequency and the C-O force constant of CO adsorbed on metals are lower than those of free CO.

The standard picture used to describe the effects of electron-transferring species upon CO chemisorption is an extension of the basic Blyholder model. Electropositive impurities donate charge to the metal. This excess charge is partially accommodated in increased π-back-donation to the $2\pi^*$ orbitals of CO. This increases the metal-CO bond strength, while decreasing the C-O bond strength. Opposite effects are expected for coadsorption with electronegative impurities. In a few coadsorption cases, this general picture has been to some extent substantiated by calculations with different quantum-chemical methods [82-89].

Theoretical work has been undertaken to address directly the predicted magnitude of the near surface electronic perturbations by impurity atoms. Early work was concentrated on the indirect interactions between adsorbates which occur via the surface conduction electrons [90-92]. These calculations suggested that atom-interactions through several lattice spacings can occur. Recent theoretical studies have expressly addressed the surface electronic perturbations by sulfur [93] as well as by Cl, P and Li [94]. The sulfur-induced total charge density vanishes beyond the immediately adjacent substrate atom site. However, the Fermi-level density of states, which is not screened, and which governs the ability of the surface to respond to the presence of other species, is substantially reduced by the sulfur even at

nonadjacent sites. The results for several impurities indicate a correlation between the electronegativity of the impurity and its relative perturbation of the Fermi-level density of states [93,94], a result which could be very relevant to the poisoning of CO methanation by S and P as discussed above. Finally, an alternate model, which produces the same final results, involves an electrostatic, through-space (as opposed to through-metal) interaction between the charge distribution of the coadsorbed species [95,96].

Both sets of theories, that is, "through-metal" or "through-space," are consistent with adsorbate perturbations sufficiently large to effect chemically significant changes at next-nearest-neighbor metal sites. This perturbation length is sufficient to adequately explain the observed poisoning of catalytic activity by surface impurities discussed above.

III.3 Metal-support interactions and CO methanation.

The early concept of a support or a carrier was that of an inert substance that provided a means of spreading out an expensive catalyst over a large surface area. However, the support may actually modify the activity of the catalyst, depending upon the reaction and reaction conditions [10,97,98]. The oxidic support materials (e.g. La_2O_3, Cr_2O_3, ZnO, MgO, TiO_2, ZrO_2...) can favorably or adversely influence the performance of a metal in a particular catalytic process [97,98]. Titania (TiO_2) is a typical example of an "interacting" support [97,98].

Surface science methods have been applied to study the CO hydrogenation activity of nickel overlayers on the $TiO_2(100)$ surface [99]. Results of ultraviolet photoelectron spectroscopy indicate that there is an electron transfer from $TiO_2(100)$ to Ni when Ni is deposited onto a reduced $TiO_2(100)$ surface [99]. When the $Ni/TiO_2(100)$ surface was used as a methanation catalyst, the CH_4 yield varied as a function of the Ni coverage, as shown in fig. 16a. At a temperature of 190°C, an average Ni thickness of ~5Å gave optimum activity. An Arrhenius plot of the specific rate of methane formation over the 5Å Ni-covered $TiO_2(100)$ surface is included in fig. 16b. The methane yields from the $Ni/TiO_2(100)$ catalyst are 3.3-3.7 times that from a pure Ni(111) catalyst. The apparent activation energy for methane production over the $Ni/TiO_2(100)$ surface (105.5 ± 2.5 kJ/mol) is very close to that seen over Ni(111) (111.8 ± 3.8 kJ/mol) [99].

A study of the methanation activity of a Ni(111) surface containing controlled amounts of TiO_x (x~1.0-1.5), showed that the nickel catalyst is optimally promoted at a titanium coverage of ~0.1 monolayer, displaying an activity and product distribution similar to those seen over 8Å Ni-covered $TiO_2(100)$ catalysts [100]. The fact that $TiO_x/Ni(111)$ and $Ni/TiO_2(100)$ are so similar in their catalytic behavior, suggests [100] that in high-surface area Ni/TiO_2 catalysts, TiO_x species diffuse from the support material to the nickel. Dispersal of the oxide on the metal and the formation of nickel-titanium bonds modify the catalytic properties of the surface.

IV. CO OXIDATION

IV.1 CO Oxidation by O_2

The catalyzed oxidation of CO by O_2 ($2CO + O_2 \rightarrow 2CO_2$) is an important process in the pollution control of combustion products. Currently, the removal of CO as CO_2 from automobile exhaust is accomplished by catalytic converters which employ a supported Pt, Pd and Rh catalyst. The relative simplicity of CO oxidation makes this reaction an ideal model system of a heterogeneous catalytic reaction. Each of the mechanistic steps (adsorption and desorption of the reactants, surface reaction, and desorption of products) has been probed extensively under UHV conditions with the modern techniques of surface science [101]. At UHV pressures, the reaction proceeds through a Langmuir-Hinshelwood mechanism involving adsorbed CO and O. The surface of the catalyst is almost entirely covered by CO, and the reaction rate is determined by the rate of CO desorption. The observed activation energy is close to the binding energy of adsorbed CO. Depending on the relative partial pressures of the reactants, self-sustained kinetic oscillations has been observed for CO oxidation on Pt [102-104] and Pd [105] single-crystal surfaces that show reconstructive phase transitions. Many of the reaction parameters determined in UHV can be applied directly to the kinetics at higher pressures [106]. In this section, we review studies dealing with the catalytic oxidation of CO by O_2 over Rh, Ru, Pt, Pd and Ir single-crystals under high pressure reaction conditions.

IV.1.1 Rh(100) and Rh(111) Surfaces

Figure 17a compares the CO oxidation rates measured over single crystals of Rh with those observed on supported Rh/Al_2O_3 catalysts [106,107]. It is clear that there is an excellent agreement between the model and supported systems in both the specific reaction rates and apparent activation energies (109 kJ mol^{-1} for Rh(111) and Rh(100) vs. 125.5 kJ mol^{-1} for Rh/Al_2O_3). These results indicate that the kinetics of CO oxidation on Rh is not sensitive to changes in catalyst surface morphology. Under the conditions of Fig. 17a, the surfaces are predominantly covered with CO so that the reaction is limited by the adsorption rate of oxygen [106,107]. As the temperature is increased, the reaction rate increases because more vacant sites are available for oxygen adsorption as a result of the higher CO desorption rate. In Fig. 17a the CO oxidation rate increases with temperature following an apparent activation energy very similar to that for CO desorption.

Figures 17b and 17c show the dependence of the rate of CO oxidation over Rh(111) on the partial pressures of CO and O_2 [106,107]. The behavior of the reaction can be analyzed by using a kinetic model established from surface science studies of the interactions of CO and O_2 with Rh [106]. In this model the mechanism of CO oxidation follows the sequence:

$$CO_g = CO_a \qquad\qquad (15)$$

$$O_{2,g} = 2O_a \qquad\qquad (16)$$

$$CO_a + O_a \rightarrow CO_{2,g} \qquad\qquad (17)$$

41

The corresponding expression for the rate of CO oxidation is:

$$r_{CO2} \approx \frac{2k_{O2,a}}{k_{COa}} \cdot k_{COd}(T) \cdot \frac{P_{O2}}{P_{CO}} \qquad (18)$$

where k_{COa}, $k_{O2,a}$ and k_{COd} (T) are the rate constants for adsorption and desorption of CO and O_2. Equation (18) is in excellent agreement with the experimental results of Figs. 17b and 17c. The reduction in catalytic activity seen in Fig. 17c for P_{O2} > 200 Torr is a consequence of an increase in the coverage of atomic oxygen on the Rh(111) surface [107]. For these cases, it appears that appreciable coverages of oxygen effectively poison the adsorption of CO.

IV.1.2   Ru(001) Surface

Specific rates of CO oxidation (molecules of CO_2 produced per surface site per second) over Ru(001) are plotted in Arrhenius form in Fig. 18a [108]. The good agreement between the results on the unsupported single crystal and those obtained on the supported catalysts attest to the appropriateness of the model. Linear Arrhenius behavior is observed below ~550K yielding an activation energy of 81.6 kJ/mol.

The effects of variations in the partial pressures of CO and O_2 upon the reaction rate are complex (see Fig. 18) [108]. At low CO partial pressures, the rate dependence is approximately positive first order in CO. This changes to negative first order at CO partial pressures above ~16 Torr. At low oxygen partial pressures (Fig. 18c), the oxidation reaction is positive order in O_2. The slope of the curve changes for O_2 pressures above ~ 4

42

Torr, becoming zero order in O_2. Post-reaction surface analysis indicate that the optimum rate of CO oxidation on Ru(001) is observed when the surface is covered by almost a monolayer of oxygen [108]. This contrasts with the case of Rh catalysts on which the optimum activity was obtained for surfaces essentially free of oxygen adatoms [107].

IV.1.3 Pt(100) Surface

The CO_2 formation rate over Pt(100) as a function of inverse temperature is shown in Fig. 19 and compared to data obtained on a Pt/SiO$_2$ catalyst [109]. The structure insensitivity of the reaction is evidenced in the match between the supported, nonoriented catalyst and the single crystal. For Pt(100) the CO oxidation reaction is always positive-first-order in O_2 pressure up to an O_2:CO ratio of 150 (Fig. 20a). The reaction order in CO changes from -0.9 at 650K to ~0 at 450K (Fig. 20b). A variation in activation energy from 138.5 to 54.4 kJ mol^{-1} is also observed in this temperature regime [109]. This may indicate a change in reaction mechanism from the CO desorption controlled Langmuir-Hinshelwood mechanism that controls the kinetics at high temperature.

The investigation of kinetic oscillations in the catalytic oxidation of CO over Pt surfaces has attracted considerable attention during the past years. UHV studies indicate that under properly chosen conditions the rate of CO oxidation at a clean and well-defined Pt(100) surface exhibits sustained temporal

oscillations which are also reflected by periodic changes of the work function [102]. These oscillations are associated with periodic variations of the surface structure. The clean Pt(100) surface reconstructs forming a hexagonal arrangement of atoms in the top most layer. If the adsorbate coverage on this hexagonal phase exceeds a critical value, the reconstruction is removed. The driving force of the kinetic oscillations is basically the change in adsorption properties as the surface switches from one configuration into the other [102]. This mechanism cannot be used to explain the presence of kinetic oscillation on Pt surfaces that do not reconstruct under high pressure conditions [110,111]. An alternative model that involves the formation of an oxide in the near-surface region of the catalyst has been proposed [110]. In the two branches of the CO oxidation reaction, the surface is oxidized or reduced, thus changing the surface oxide coverage. This coverage determines in which of the two branches the reaction will occur [110]. The main defect of this model is the fact that Pt oxides are nonstable under reaction conditions [109]. Studies of CO oxidation over Pt(100) indicate that no strongly bound, deactivating surface oxygen species is formed [109]. Oscillatory reaction rates have been observed for CO oxidation over Pt(111), Pt(100) and Pt(13,1,1) catalysts at atmospheric pressure [111]. It appears that silicon impurities were present on the surfaces supporting the oscillations. These impurities play an important role in the oscillatory behavior by either catalyzing the formation of a Pt

oxide or by increasing the sticking coefficient of oxygen on the Pt surface [111].

IV.1.4 Pd(110) Surface

Fig. 19 displays steady-state specific rates for CO oxidation over Pd(110) and Pd/SiO$_2$ catalysts [109]. For the single-crystal the apparent activation energy is 138.6 kJ mol^{-1} at temperatures in the range between 475 and 625K. At P$_{O2}$/P$_{CO}$ ratios lower than 12, the CO oxidation reaction on Pd(110) is negative-first order in CO pressure and positive order in O$_2$ pressure, in good agreement with supported catalyst data [109]. The reaction becomes negative-first order in O$_2$ pressure and approximately first order in CO pressure for P$_{O2}$/P$_{CO}$ ratios greater than 12 [109]. Under such oxidizing conditions, a strongly bound oxygen species is formed on the Pd(110) catalyst. This strongly bound oxygen species decomposes in post-reaction TPD yielding CO$_2$, suggesting the formation of a CO$_x$ species during the reaction [109]. Deliberate oxidation of the Pd surface prior to the CO + O$_2$ reaction resulted in a rate decrease but did not affect the activation energy significantly, indicating that the oxide served merely as a simple site blocker [109].

Reaction rate oscillations have been observed for CO oxidation on Pd(110) [105]. The existence region for oscillations was determined for pressures ranging from 10^{-3} to 1.0 Torr and depended on the pressures of O$_2$ and CO and the

sample temperature. A densely packed CO structure and a strongly bound oxygen or subsurface oxygen limit the reaction at high and low rates, respectively [105]. The extension of oscillations from UHV conditions to the 1.0 Torr pressure region indicates that the mechanism responsible for the oscillations may be independent of the reactant pressure up to several Torr.

IV.1.5   Ir(110) and Ir(111) Surfaces

The structure insensitivity of the CO oxidation reaction in evidenced in the results of Fig. 19 [109]. There is a match between the rates observed on Ir(110) and Ir(111) single crystals and those for a supported Ir catalyst. Fig. 21 shows the reaction rate dependence on CO and O_2 partial pressures for Ir(111) [109]. Stoichiometric mixtures ($P_{CO}/P_{O2} = 2$) have reaction orders of -0.9 ± 0.2 in CO and 0.9 ± 0.2 in O_2. Under highly oxidizing conditions, Ir(111) shows negative-order dependence in O_2 partial pressure, indicating the presence of a strongly bound oxygen species. This species reduces the overall rate of reaction and can be detected as CO_2 desorbing at ~670K in post-reaction temperature-programmed desorption [109].

IV.1.6 Summary

The results discussed above demonstrate the structure insensitivity of the CO oxidation reaction. The observed activation energies and reaction orders are summarized in Table II. For CO + O_2 mixtures close to stoichiometric, in general,

the reaction rate is independent of total pressure, first-order in O_2 pressure and negative-first-order in CO pressure. This behavior is consistent with a Langmuir-Hinshelwood mechanism involving adsorbed CO and O, with the reaction rate governed by the desorption of CO [106]. On Rh, Pd, and Ir catalysts, increases in the O_2/CO ratios result in an eventual decrease in the rates of CO oxidation, as a consequence of the formation of an oxide-like species over the surfaces. In contrast, on Ru(001) the oxide is substantially more active than the clean substrate.

IV.2 CO Oxidation by NO

IV.2.1 Rh(100) and Rh(111) Surfaces

Supported Rh catalysts are commonly used for controlling pollution from combustion products such as CO and NO. CO oxidation (and NO reduction) occurs mainly through the overall reaction:

$$CO + NO \rightarrow CO_2 + N_2 \qquad (19)$$
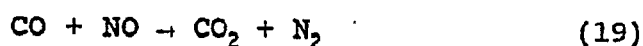
This catalytic process has been the subject of a large body of research in recent years [106,112,113].

Arrhenius plots for CO oxidation by NO on Rh(100) and Rh(111) are shown in Fig. 22 for equal partial pressures of CO and NO (8.0 Torr) [112]. Significantly different activation energies (Rh(111): 121.4 kJmol^{-1}; Rh(100): 100.5 kJmol^{-1}) and specific activities are observed on the two surfaces, indicating that this reaction is sensitive to the geometric structure of the catalyst surface [112]. the CO + NO reaction exhibits

47

substantially different kinetic behavior between supported Rh/Al$_2$O$_3$ and Rh(111) [106].

The dependence of the reaction rate on the partial pressures of the reactants is shown in Fig. 23 [112]. The data indicate little if any variation on the rate with changing CO pressures on either surface. Similar NO pressure independence is observed over the two surfaces for NO pressures below 20 Torr. On Rh(111), the reaction rate becomes positive order at higher NO partial pressures. This behavior is in excellent agreement with the predictions of a kinetic model based on the following set of elementary processes [106]:

$$CO_g \rightleftharpoons CO_a \qquad\qquad (20)$$

$$NO_g \rightleftharpoons NO_a \qquad\qquad (21)$$

$$NO_a \rightarrow N_a + O_a \qquad\qquad (22)$$

$$NO_a + N_a \rightarrow N_2 + O_a \quad (\delta\text{-}N_2) \quad (23)$$

$$2N_a \rightarrow N_{2,g} \qquad (\beta\text{-}N_2) \qquad (24)$$

$$CO_a + O_a \rightarrow CO_{2,g} \qquad\qquad (25)$$

For Rh(111) the model suggest that the surface is predominantly covered by adsorbed N-atoms and NO, and the rate is limited by the surface reaction of N$_a$ (β-N$_2$ formation) which frees up adsorption sites on the surface for the other reactants [106,112]. The similarity between the activation energy for reaction (24) (~130 kJ mol^{-1}) and the apparent activation energy for the overall reaction (~121 kJ mol^{-1}) supports this conclusion [106,112]. The reaction on Rh(100) may be rate-limited by δ-N$_2$.

formation due to the greater activation energy for β-N_2 formation on this surface [112].

V. ETHYLENE EPOXIDATION

The catalytic oxidation of ethylene to ethylene epoxide ($2C_2H_4 + O_2 \rightarrow 2C_2H_4O$) is a several-billion-dollar per year industry [114], providing the necessary intermediate in the synthesis of ethylene glycol, which is used in polyester and antifreeze production. The most common catalyst consists of reduced silver particles dispersed on α-Al_2O_3 [115,116]. Cesium is added to the catalyst as a promoter. In addition, chlorinated hydrocarbons are usually present in the reactant feed in order to improve the selectivity of the catalytic process toward ethylene epoxide production. In the presence of oxygen, ethylene can react to yield ethylene epoxide or undergo total combustion producing CO_2 and H_2O:

$$C_2H_4 + O_2 \xrightarrow{k_1} C_2H_4O$$
$$k_2 \searrow \qquad \nearrow k_3 \qquad\qquad (26)$$
$$CO_2 + H_2O$$
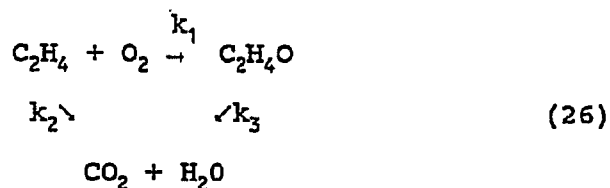
The heats of reaction, per mole of ethylene, are $-\Delta H_1 = 146$ kJ/mol and $-\Delta H_2 = 1320$ kJ/mol [10]. The oxidation of ethylene to ethylene epoxide over Ag is the simplest example of kinetically-controlled selective catalytic reactions.

V.1 Kinetics over Ag(110) and Ag(111) catalysts

Recent studies [117] show that turnover rates for ethylene oxidation over the (110) and (111) planes of Ag differ by a factor of only 1.8, a result indicative of structure insensitivity [117,118]. The Ag(111) and (110) single-crystal surfaces are excellent kinetic models of high-surface-area supported Ag catalysts, with virtually identical activation energies and reaction orders with respect to ethylene and oxygen pressures.

Fig. 24 shows steady-state rates of C_2H_4O and CO_2 production as a function of temperature, in Arrhenius form, for P_{Et} = 20 Torr and P_{O2} = 150 Torr on the clean Ag(110) surface [8]. Shown for comparison is the specific rate of C_2H_4O production over a silica-supported Ag catalyst (from ref. [119]). The apparent activation energy for C_2H_4O production, while varying with temperature from 93.8 kJmol^{-1} near 450K to 22.1 kJmol^{-1} near 580K, is virtually identical on Ag(110) and on the high-surface area catalyst. The activation energies for C_2H_4O and CO_2 production are quite similar, a finding that indicates a common rate-limiting step [8]. The specific activity of Ag(110) is about 100 times higher than those of supported Ag catalysts [120]. A simple and therefore appealing explanation for the discrepancy in turnover rates is the contamination of the supported silver by impurities [117,118,120].

Fig. 25a illustrates the effect of O_2 pressure upon the steady-state rates of C_2H_4O and CO_2 production over Ag(110) at

490K and P_{Et} = 4.1 Torr [8]. At low P_{O2}, the reaction orders in P_{O2} approach unity. When P_{O2} exceeds about $8P_{Et}$, the orders in P_{O2} begin to approach to zero. The selectivity increases with P_{O2}, reaching a maximum value at $P_{O2} \geq 8P_{Et}$. Very similar trends have been observed for supported Ag catalysts [8]. Also shown in Fig. 25a is the coverage of atomic oxygen on the Ag(110) catalyst after reaction conditions [8]. Oxygen coverages were measured by rapidly (17-45s) transferring the single crystal at reaction temperature from a reaction chamber to an UHV chamber for surface analysis. It has been argued that this method underestimates the oxygen coverages during the reaction [121]. No adspecies containing atoms other than C, O, H and Cl ($\theta_{Cl} < 0.02$) were observable by surface analysis. Measurements of the surface concentration of weakly bound species such as $C_2H_{4,a}$ and $O_{2,a}$ was not possible because they desorb during transfer of the crystal into the UHV chamber.

Fig. 25b displays the effect of ethylene pressure upon the rates of C_2H_4O and CO_2 production on Ag(110) for P_{O2} = 150 Torr and T = 490K [8]. At very low P_{Et}, the reactions are near first order in P_{Et}. As P_{Et} increases, the order decreases and finally drops to zero as the surface saturates in ethylene.

There is not general agreement about the mechanism for ethylene epoxidation on silver. Arguments concerning the roles of various forms of oxygen on the surface of silver remain the subject of much debate [115-127]. Recent isotopic tracer experiments [124] indicate that ethylene can react with adsorbed

51

atomic oxygen to give the corresponding epoxide, provided that

subsurface oxygen is present. Once the adsorbed atomic oxygen

has been formed, the rate-limiting step for epoxidation is the

insertion of this oxygen into the C-C double bond [124,125]. The

rate-limiting step for combustion is probably a C-H bond

activation, although C-C bond activation cannot be definitely

excluded [125]. Subsurface oxygen seems to be necessary for

adsorbed oxygen to react to epoxide [124]. Quantum-chemical

calculations (using model clusters of the Ag(110) surface and the

Hartree-Fock-Slater Xα method) [125] show that the presence of

subsurface oxygen reduces the bond energy between silver and

adsorbed atomic oxygen, and converts the repulsive interaction

between oxygen adatoms and gas-phase ethylene into an attractive

one, thus making possible the epoxidation reaction. Experiments

using Ag(111) as a catalyst [122] have lent support to the view

that atomic oxygen reacts with ethylene to form both ethylene

epoxide and CO_2. Oxygen dissolved on Ag(111) promotes selective

oxidation [122].

V.2   Chlorine promotion of Ag(110) and Ag(111) surfaces

Kinetic data for Ag(110) [128,129] and Ag(111) [121,130]

indicate that adsorbed chlorine reduces the activity and

increases the selectivity of these surfaces toward ethylene

epoxidation. Typical results are presented in Fig. 26. The

effects of chlorine addition are very similar on Ag(111) and

Ag(110). Fig. 27 summarizes the results of a series of

experiments where the influence of chlorine coverage upon the kinetics of ethylene oxidation on Ag(110) was determined [129]. The fact that the kinetic parameters for full combustion essentially track those for epoxidation suggest that a common adsorbed intermediate is formed in the rate-determining step of both pathways, and that the selectivity is only determined subsequent to this step by the branching ratio of two relatively rapid competing reactions available to this intermediate [129]. Chlorine improves the selectivity by altering the branching ratio to favor ethylene epoxide. It has been proposed [129,130] that this occurs mainly via an ensemble effect, in which the chlorine blocks the Ag sites that are necessary for fragmentation and full combustion of the intermediate. An alternative model [121-123] suggests that the role of Cl as a promoter can be rationalized in terms of the way in which it alters the electron density on O_a. By competing for metal electrons and thus reducing the amount of negative charge on O_a, adsorbed chlorine favors electrophilic addition of O_a to ethylene (leading to C_2H_4O formation) and disfavors H-stripping by O_a (which would lead to combustion).

V.3 Cesium promotion of Ag(111)

The effects of Cs pre-coverage upon the steady-state rates of CO_2 and C_2H_4O production over Ag(111) are shown in Fig. 28 [131]. Under the experimental conditions of these measurements, Cs always tends to decrease the activity for C_2H_4O and CO_2 production, with an increase in the selectivity toward C_2H_4O when

θ_{Cs} exceeds 0.15. Somewhat different trends were observed when the reaction was carried out at 500K with a 1:1 mixture of C_2H_4 and O_2 at a total pressure of 10 Torr [132,133]. In this case, the activity and selectivity for C_2H_4O production were slightly enhanced as Cs was added, until a maximum was reached at $\theta_{Cs} \approx$ 0.25. For $\theta_{Cs} > 0.3$, an increase in the coverage of Cs induced a reduction in selectivity and activity.

The thermal stability of Cs on Ag is greatly enhanced under reaction conditions due to the formation of a surface cesium "oxide" ($\sim CsO_3$) which exists in islands that show a $(2\sqrt{3} \times 2\sqrt{3})R30^\circ$ LEED pattern [131]. The formation of this "oxide" is very rapid and can also be accomplished with small doses of O_2 gas to Cs/Ag(111) in UHV conditions. It decomposes near 600K in UHV, yielding nearly simultaneous desorption of O_2 and Cs gas.

It has been proposed that the principal role of Cs is in the secondary chemistry, where it acts to supress the isomerization (and hence the further oxidation) of ethylene epoxide [122b].

VI.   THIOPHENE HYDRODESULFURIZATION

Organosulfur compounds are common impurities in crude oil. Due to a variety of reasons [10], it is necessary to reduce the sulfur content of petroleum fractions. The process used for this purpose is catalytic treatment with hydrogen (hydrodesulfurization) to convert the various sulfur compounds present in the oil to hydrogen sulfide [10,134]. The most frequently used catalyst is a mixture of cobalt and molybdenum on a γ-alumina

support, which is sulfided before use. The ratio of Mo/Co is always considerably greater than 1. The hydrodesulfurization (HDS) of thiophene is often used to test the activity of Co-Mo/Al$_2$O$_3$ catalysts [134]. The main reaction pathway is:

thiophene + 3H$_2$ → H$_2$S + butene (mixed isomers)   (27)
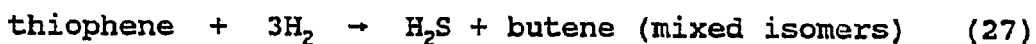
In recent years the adsorption and decomposition of thiophene on metal surfaces have been extensively studied in UHV [135-141]. The kinetics and mechanism of thiophene hydrodesulfurization at atmospheric pressures have been investigated over single-crystal surfaces of Mo and Re [142-146].

VI.1 Kinetics on Mo Surfaces

The catalytic hydrodesulfurization of thiophene over Mo(100) can be readily performed [142,144]. An Arrhenius plot of the appearance rates of each of the products is shown in Fig. 29 . The curves for the butenes all have similar temperature dependence. Arrhenius behavior is only observed for the rate of production of butadiene (apparent activation energy = 60.3 ± 8 kJ/mol [144]). The reaction product distribution on Mo(100) is compared in Fig. 29b with that observed over a MoS$_2$ catalyst [144]. It is clear that the two distributions are almost identical, suggesting that over both surfaces the reaction proceeds via the same mechanism.

Fig. 30 illustrates the dependence of the reaction rates for butane, the butenes and butadiene on the hydrogen and thiophene partial pressures [144]. The dependence among the three butene isomers shows very little variation. The rate dependence on P_{H2} is approximately 1, 1/2 and 0 for butane, the butenes and butadiene, respectively. The rate of butadiene production has a first-order dependence in thiophene pressure, while the hydrogenated products show only very weak dependence.

TPD and HREELS experiments investigating the surface chemistry of thiophene on Mo(100) [138] indicate that the mechanism for molecular decomposition changes as a function of adsorbate coverage. At low coverages, the molecule adsorbs parallel to the surface. C-S bonds are broken, and subsequent dehydrogenation of the remaining hydrocarbon fragments takes place in the 100-340K temperature range [138]. At saturation coverages, the thiophene molecules chemisorb in a perpendicular configuration. Sequential dehydrogenation starts with C-H bond breaking in one of the α positions at ~ 230K. The loss of a β-hydrogen follows at about 350K, when a stable intermediate forms and does not react any further until heating above 550K. Full dehydrogenation is achieved at ~ 700K, leaving only carbon and sulfur on the surface [138]. Mo(110) exhibits reactivity similar to Mo(100), suggesting that the decomposition of thiophene over molybdenum is not sensitive to the surface structure [137].

The active catalytic surface of a Mo(100) single crystal during thiophene HDS is deficient of hydrogen and covered with

56

adsorbed carbon from thiophene decomposition [143,144].

Deposition of atomic sulfur onto the catalyst surface does not

occur during desulfurization of thiophene. On Mo(100), the rate

of hydrogenation of adsorbed sulfur to H_2S is much lower than the

rate of thiophene hydrodesulfurization [145]. These results are

consistent with a mechanism in which the desulfurization occurs

via either an intramolecular step (in which the sulfur atom is

hydrogenated by atoms originating from the thiophene molecule) or

a direct hydrogenolysis of C-S bonds to form H_2S [144,145]. The

thiophene HDS reaction appears to proceed through initial

desulfurization to yield butadiene, followed by hydrogenation

reactions producing butenes and butane [144].

Fig. 31 shows the thiophene HDS activities for three low-

Miller-index planes of molybdenum (P_{Th}= 3.0 Torr, P_{H2}= 780 Torr,

T= 613K) [146]. Although the surfaces have very different

roughness exposing atoms with different coordination number, the

rate of thiophene HDS is very similar on all of them. Under

reaction conditions the Mo single crystals are covered with a

layer of carbon [146]. This overlayer blocks the influence of the

metal surface structure on the catalyst activity.

VI.2 Kinetics on Re Surfaces

The rates of thiophene HDS over four faces of rhenium are

displayed in Fig. 32 [146]. In contrast to the case of Mo

surfaces on which the reaction is structure insensitive, the Re

single crystals show a six fold increase in activity on going

from the hexagonal close-packed Re(0001) surface to the more corrugated Re($10\bar{1}0$) surface. The interaction between thiophene and rhenium is not moderated by an overlayer of carbon as was found with molybdenum [146]. The trend of increasing HDS activity of the Re surfaces ((0001)<($11\bar{2}1$)<($11\bar{2}0$)<$10\bar{1}0$)) does not follow the increase in surface openness ((0001)<($10\bar{1}0$)<($11\bar{2}0$)<$11\bar{2}1$)). This fact indicates that surface openness is not the determining factor in catalyst activity [146]. It appears that the Re($10\overline{10}$) and Re($11\bar{2}0$) surfaces expose a particular configuration of active sites that is not present in a smooth surface such as Re(0001) or in a very open surface such as Re($11\bar{2}1$).

VII. ALKANE HYDROGENOLYSIS

Hydrogenolysis of an alkane is the cleavage of a C–C bond accompanied by hydrogenation to form two hydrocarbon molecules from one. The hydrogenolysis of paraffins is of great importance in petroleum processing in which it is sometimes a desired reaction, as in commercial hydrocracking, and sometimes not desired, as in catalytic reforming [10]. The most active metallic catalysts are those in group VIII [10,147]. The distribution of primary products from hydrogenolysis varies substantially with the nature of the metal. In addition, the specific activity and selectivity of the catalysts have been found to be sensitive to the average metallic particle size.

The hydrogenolysis reactions usually require a relatively large ensemble or group of active sites on the surface of the

catalyst [41,42]. Alkane hydrogenolysis can be selectively suppressed by removing or poisoning a fraction of the active sites. This approach has been applied in the design of industrial reforming catalysts [10,41,142]. For example, the selectivity of Ni for dehydrogenation versus hydrogenolysis can be greatly increased by adding an inactive metal (Cu) to form an alloy.

Metal-single crystals offer unique possibilities in the study of the effects of surface structure and composition upon alkane hydrogenolysis. In the present section we review works dealing with the hydrogenolysis of small hydrocarbons over well-defined monometallic and bimetallic surfaces. As a result of this type of studies, a fundamental understanding of the electronic and structural properties responsible for the catalytic behavior of metal systems in alkane hydrogenolysis is beginning to evolve.

VII.1 Ethane Hydrogenolysis

Ethane hydrogenolysis ($C_2H_6 + H_2 \rightarrow 2CH_4$) is the most extensively studied cracking reaction [10,147]. The activity for ethane hydrogenolysis depends markedly on the size of metal catalyst particles and upon the nature of the metal [147]. This reaction therefore has been described as structure sensitive.

VII.1.1 Monometallic Surfaces
A. Ni(100) and Ni(111)

Fig. 33 shows the specific reaction rate for methane formation from ethane over Ni(100) and Ni(111) catalysts [148].

The values shown are for a P_{H2}/P_{C2H6} ratio of 100 and a total pressure of 100 Torr. At a given temperature the rate of methane production over an initially clean crystal was extremely constant with no apparent induction period [148]. The carbon level during reaction remained constant at a submonolayer coverage [148]. In Fig. 33 it is evident that the activity of the (111) surface toward ethane hydrogenolysis is considerably less than that observed for the (100) surface. The activation energy associated with the (111) data (192.6 kJ/mol) compares much more favorably with results for Ni/SiO$_2$ [149] than that for the (100) data (100.5 kJ/mol). The high surface area catalyst is expected to contain metal crystallites exposing predominantly (111) faces [148,149].

The differences in the spacing between high coordination bonding sites on the Ni(100) and Ni(111) surfaces could account for the differences in activity [148]. For the (100) surface the spacing between the four-fold hollow sites is ~2.5Å . The C-C bond length of an adsorbed intermediate is expected to be from 1.3 to 1.5Å (the range of C-C bond lengths between acetylene and ethane). Upon adsorption of ethane on Ni(100), the C-C bond cannot remain intact when the carbon atoms bond to the preferred high coordination sites of the surface. The situation is different, however, for Ni(111). In this case, the 1.4Å spacing between the high coordination sites is ideally suited for maintaining the C-C bond intact while bonding each carbon to a three-fold hollow site. An additional contribution to the

60

differences in hydrogenolysis activity between Ni(100) and Ni(111) can come from differences in the electronic properties of these surfaces [148]. If backbonding from the metal to the unfilled σ^* levels of ethane is an important first step toward C-C bond scission in ethane, then the (100) surface should be more active than the (111), given that the appropriate Ni orbitals for such backbonding are more available in the case of the (100) surface [148,150].

Adsorbed sulfur induces a large decrease ($\sim$ 90% at θ_s= 0.1) in the rate of ethane hydrogenolysis on Ni(100) [151]. The experimental data suggest that electronic effects, rather than ensemble requirements, dominate the poisoning mechanism.

B. Ru(001) and Ru(1,1,10)

The temperature dependence of the rate of CH_4 formation from ethane hydrogenolysis over Ru(001) [152] and Ru(1,1,10) [153] is plotted in Arrhenius form in Fig. 34 . The Ru(1,1,10) surface has (001) terraces which are five-atoms wide and separated by (110) steps in a zig-zag form close to a kink structure [153,154]. The apparent activation energies in Fig. 34 (Ru(001) $\approx$ 84kJ/mol at T= 500-570K; Ru(1,1,10) = 92kJ/mol at T= 475-522K) are quite smaller than the value reported for silica supported Ru catalysts (134kJ/mol [155]).

Fig. 35 shows the rate of ethane hydrogenolysis over Ru(001) as a function of H_2 partial pressure [152]. In agreement with studies on Ru/SiO$_2$ [155] and Ru(1,1,10) [153], the reaction is

61

negative order with respect to hydrogen for partial pressures of H_2 above 40 Torr. The reaction order with respect to ethane was observed to be +0.85 on Ru(001) [152], +0.55 on Ru(1,1,10) [153] and +0.8 on Ru/SiO$_2$ [155]. The order of the hydrogenolysis reaction with respect to the two reactants reflects the ability of hydrogen to compete more favorably for adsorption sites on the catalysts [152]. In Fig. 35 the change to positive order at low H_2 pressures indicates the conditions at which the surface concentration of hydrogen falls below the critical optimum value. This surface depletion of hydrogen causes a departure of the reaction rate from linear Arrhenius behavior at high reaction temperatures (see Fig. 34a).

Sulfur adatoms largely reduce the rate of ethane hydrogenolysis over Ru(001) ($\sim$ 50% at θ_s= 0.1 and $\sim$ 70% at θ_s= 0.5; T= 500-575K, P_{total}= 100 Torr, H_2/C_2H_6= 99) [152]. A study of sulfur poisoning of Ru(1,1,10) [153] revealed that atoms in step sites of this surface are much more active for ethane hydrogenolysis than atoms in the (001) terraces. The low coordination number of the Ru atoms in the step sites makes them more reactive in C-C bond breaking.

C. Ir(111) and Ir(110)-(1x2)

Specific rates of ethane hydrogenolysis over Ir(111) and Ir(110)-(1x2) are shown in Fig. 36 [156]. The clean Ir(110) surface reconstructs into a (1x2) superstructure [157], which contains a large fraction (25%) of low coordination number edge

atoms (C_7). The (1x2) reconstruction is expected [156] to be
stable under reaction conditions. For temperatures below ~ 550K,
the (111) surface is more active than the (110)-(1x2), whereas,
above 550K, the opposite is true. In the linear Arrhenius regime
(T < 550K) the rate constants ($k=A \exp(-E_a/RT)$) on the two
surfaces differ considerably [156]: $E_a \approx$ 147 kJ/mol and A=
$1x10^{13}$ molecules site^{-1} s^{-1} for Ir(111), and $E_a \approx$ 205 kJ/mol and
A= $6x10^{18}$ molecules site^{-1} s^{-1} for Ir(1110)-(1x2).

Post-reaction surface characterization by AES indicated the
presence of a submonolayer carbonaceous residue ($\theta_C \approx$ 0.2) on the
Ir single crystals [156]. On both surfaces ethane hydrogenolysis
was approximately first-order in P_{ethane}, while the order in P_{H2}
varied from -1.5 over Ir(111) to -2.5 over Ir(110)-(1X2) [156].
The dependence of the rate of ethane hydrogenolysis with respect
to the partial pressures of the reactants was analyzed using a
mechanistic scheme in which the rate-limiting step involves an
irreversible C-C bond cleavage in a partially dehydrogenated
hydrocarbon fragment:

$$C_2H_{6,g} \; = \; C_2H_{x,a} \; + \; (6-x)H_a \qquad (28)$$

$$H_{2,g} \; = \; 2H_a \qquad (29)$$

$$C_2H_{x,a} \; \xrightarrow{\text{slow}} \; CH_{y,a} \; + \; CH_{z,a} \qquad (30)$$

$$CH_{z,a} \text{ (or } CH_{y,a}) + nH_a \; \xrightarrow{\text{fast}} \; CH_{4,g} \qquad (31)$$

According to this model the intermediates preceding C-C bond breaking are C_2H_4 on Ir(111) and C_2H_2 on Ir(110)-(1x2). This difference can be explained by arguments based on structural considerations. Under the (1x2) reconstruction the Ir(110) surface is very open, exposing sites with different coordination number (see Fig. 36). It is quite conceivable that on this surface an extensively dehydrogenated hydrocarbon fragment may be formed, whereas on the essentially flat Ir(111) surface, its formation is not energetically favorable [156].

D. Pt(111)

Values of 153.2 ± 13 kJ/mol [158] and 144 ± 3 kJ/mol [159,160] have been reported for the apparent activation energy of ethane hydrogenolysis on Pt(111). Both values are considerably smaller than the activation energy of ~ 226 kJ/mol observed on alumina- and silica- supported platinum catalysts [147,161]. Under reaction conditions the Pt(111) surface is covered by a submonolayer of a carbonaceous residue [158,159]. A comparison of deuterium exchange rates with hydrogenolysis rates for ethane on Pt(111) indicates that C-H bond scission is rapid relative to C-C bond scission [159], suggesting that C-C bond breaking dominates the kinetics of ethane hydrogenolysis over this surface. The reaction proceeds with orders in C_2H_6 and H_2 pressures of 1 and -1.8, respectively [158]. An analysis of the dependence of the hydrogenolysis rate with respect to the partial pressures of the reactants indicates that the surface hydrocarbon fragment

64

preceding C-C bond breaking is C_2H_4 or C_2H_3. It has been proposed that ethylidine ($\equiv$C-CH$_3$) is the precursor to C-C bond cleavage [158,159].

E. Re(001)

The rate of ethane hydrogenolysis on Re(001) was examined at P_{H2}= 100 Torr, P_{ethane}= 10 Torr and T= 573-623K [160]. The reaction exhibited linear Arrhenius behavior, with an apparent activation energy of 75.3 ± 4.2 kJ/mol. At 573K the initial rate of methane formation was 0.55 molecules site^{-1} s^{-1}. The rate could be increased up to 1.8 molecules site^{-1} s^{-1} by roughening the surface with argon ion sputtering and no annealing. This fact indicates that ethane hydrogenolysis is structure sensitive on Re surfaces. Post-reaction surface analysis revealed a carbonaceous layer on the Re(001) catalyst [160]. The accumulation of carbonaceous deposits was fairly insensitive to temperature and hydrogen partial pressure.

F. W(100)

Methane was produced catalytically when a W(100) crystal was heated at temperatures between 513 and 613 in a mixture of H_2 (100 Torr) and ethane (1 Torr) [162]. After a period of several minutes during which little or no methane was formed, constant turnover frequencies for the reaction of ethane were observed. Post-reaction surface analysis indicated that the true catalyst was a monolayer of carbide which was formed on the W(100) surface

on exposure to the reactants. When the crystal surface was carburized before reaction, no induction period was detected in ethane hydrogenolysis.

The hydrogenolysis reaction was approximately first-order in ethane and half-order in H_2, displaying an apparent activation energy of 113 kJ/mol [162]. This activation energy is identical to that reported on evaporated tungsten films [163].

G.   Summary

Table III shows specific activities and apparent activation energies for ethane hydrogenolysis on several metal single-crystal catalysts. The activation energies vary between 75 and 210 kJ/mol. In general, surfaces presenting activation energies below 100 kJ/mol show the highest catalytic activities. A comparison of the turnover frequencies (TOF) at P_{H2}= 100 Torr, P_{ethane}= 1 Torr and T= 575K gives the following order of catalytic activity: Ir(110)-(1x2) > Ir(111) > Ru(001) > Ni(100) > Re(001) > Ni(111) > W(100) > Pt(111). In this series the TOF varies from ~ 0.001 CH_4 molecules site^{-1} s^{-1} on Pt(111) [158] to ~ 2 CH_4 molecules site^{-1} s^{-1} on Ir(110)-(1x2) [156].

The studies reviewed in this section show unambiguously that ethane hydrogenolysis can be classified as a structure sensitive reaction. For a given metal, open planes show higher catalytic activity than the close-packed face. The reaction occurs in the presence of a carbonaceous layer on the surface of the catalyst. The fraction of the crystal surface covered by carbon under

66

reaction conditions depends on the nature of the metal: $\theta_c \leq 0.2$ for Ni and Ir, $\theta_c \approx 0.5$ for Pt, and $\theta_c = 1$ for W(100).

VII.1.2   Bimetallic Surfaces

A.   Ni/W(110) and Ni/W(100)

Fig. 37a shows the turnover frequencies for methane formation from ethane hydrogenolysis over different Ni/W(110) surfaces [51]. The reaction rate decreases with increasing Ni coverage. Arrhenius behavior is observed in all the cases, with an apparent activation energy independent of Ni coverage (~ 91 kJ/mol [51]). Data for ethane hydrogenolysis on Ni/W(100) catalysts are shown in Fig. 37b [51]. In contrast to the results on W(110), the turnover frequencies on Ni/W(100) are independent of Ni coverage. As discussed above, kinetic studies show much higher rates for ethane hydrogenolysis on Ni(100) than on Ni(111). This difference can be attributed to the spacing of the high-coordination sites on the crystals [148]. The large spacing on Ni(100) (~2.5Å) facilitates the breaking of the C-C bond in adsorbed ethane. This suggests that if the separation between the Ni atoms is sufficiently large, the rate of ethane hydrogenolysis will be large and independent of Ni structure. It appears that this is the case for Ni/W(100) [51], where the distance between high-coordination sites is ~ 2.7Å and the rates are independent of Ni coverage.

Also shown in Fig. 37b are data from a Ni(100) catalyst [148] and the rates from Ni/W(110) in the limit of zero Ni

coverage. For all these systems, the reaction rates and activation energies are essentially identical. This suggests [51] that the reaction mechanism on Ni/W(110) is similar to the mechanism on Ni(100) and Ni/W(100) and that the proportion of active metal atoms is changing as a function of Ni coverage. A plausible model is that only isolated and/or low coordination (island edge) atoms exhibit high activity in Ni/W(110). As zero coverage is approached, the proportion of low-coordination Ni atoms increases, and the hydrogenolysis rate gets closer to that of the "open" Ni/W(100) surface.

B. Ni/Pt(111)

Specific rates of ethane hydrogenolysis as a function of Ni coverage on Pt(111) are shown in Fig. 38 [158]. The reaction rate increases monotonically as Ni is added to the Pt(111) surface, until a maximum is reached at ~ θ_{Ni}= 1.3 . The catalytic activity of a Pt(111) surface with the equivalent of a monolayer of Ni atoms is ~ 30 times higher than that seen for clean Pt(111). An analysis of the increase in the rate of hydrogenolysis with Ni coverage suggests an ensemble requirement of two or three Ni atoms for this reaction [158]. For Ni coverages in the range between 1.2 and 3 ML, the catalytic activity of the Ni/Pt(111) surface is lower than that reported for Ni(100) under similar experimental conditions (~ 0.15 CH_4 molecules site^{-1} s^{-1} [148]) and close to that observed for Ni(111) (~ 0.05 CH_4 molecules site^{-1} s^{-1} [148]).

Independent of Ni coverage, the rate of hydrogenolysis was approximately first order in ethane pressure [158]. In contrast, the order with respect to hydrogen pressure varied as follows [158]: $\theta_{Ni} = 0$, n= -1.8 ± 0.3 ; $\theta_{Ni} = 0.4$, n= -2.1 ± 0.3 ; $\theta_{Ni} = 1$, n= -2.4 ± 0.3; and $\theta_{Ni} = 1.3$, n= -2.5 ± 0.3 . The hydrogenolysis reaction was always negative order in hydrogen partial pressure, and the dependence increased with Ni coverage. The dependence of the rate of ethane hydrogenolysis with respect to the partial pressures of the reactants indicates [158] that the hydrocarbon fragments preceding C-C bond cleavage are C_2H_4 or C_2H_3 (perhaps ethylidine) on clean Pt(111) and C_2H_2 on Pt(111) surfaces with Ni coverages of 1 and 1.3 ML. Thus, the extent of dehydrogenation of the ethane molecule on the surfaces increases with Ni coverage. This is consistent with results that show that the presence of Ni adatoms on Pt(111) enhances the capacity of this surface to dissociate ethane (C-H bond breaking) [158].

C. Re/Pt(111) and Pt/Re(001)

Specific rates of ethane hydrogenolysis on Re/Pt(111) and Pt/Re(001) catalysts are shown in Fig. 39 [160]. The addition of 0.6-1 ML of Re to Pt(111) results in surfaces with a hydrogenolysis activity much larger than that of Pt(111) or Re(001). High catalytic activity is also observed for $Pt_{<1}$/Re(001). A bimetallic surface of Re_2Pt stoichiometry was found to be the most active catalyst for ethane hydrogenolysis (approximately one order of magnitude more reactive than

Re(001)). These results show that an electronic interaction exists between the two metals resulting in a hydrogenolysis activity larger than that displayed by either monometallic component alone [160].

D. Cu/Ru(001)

Fig. 40 illustrates the effect of Cu coverage upon the rate of ethane hydrogenolysis on Ru(001) [152]. For comparison data for sulfur poisoning is also plotted. The initial slope indicates that Cu merely serves as an inactive diluent [152], blocking active Ru sites on a one-to-one basis with three dimensional cluster growth occurring at roughly a third of a monolayer. The contrast in reaction rate attenuation by Cu compared with S can be attributed to differences in relative electronegativities [152], where the more electronegative S alters the surface activity more profoundly than by a simple site blocking mechanism.

VII.2   Propane Hydrogenolysis
VII.2.1 Ir(111) and Ir(110)-(1x2) Surfaces

Compared to ethane, considerably less work has been carried out for the hydrogenolysis of propane over metal catalysts [156]. Examination of the results in Fig. 41 shows that the specific activities and apparent activation energies for propane hydrogenolysis are very similar on the Ir(111) and Ir(110)-(1x2) surfaces [156]. This suggests that the reaction mechanism on both

surfaces is the same. It has been proposed [156] that the precursor for C-C bond breaking is an adsorbed C_3H_6 species bound to the surface via two single carbon-metal bonds, which may involve more than one metal surface atom.

VII.3   Butane Hydrogenolysis

VII.3.1   Ir(111) and Ir(110)-(1x2) Catalysts

Specific rates of hydrogenolysis of n-butane over Ir(111) and Ir(110)-(1x2) are shown in Fig. 42 . On supported Ir catalysts the selectivity for n-butane hydrogenolysis is extremely dependent on the average metallic particle size [164]. Fig. 43 shows the selectivity for ethane production as a function of the mean particle diameter [156] for both the supported catalysts and the two single-crystal surfaces. The observed enhancement in the ethane selectivity with decreasing particle size is a consequence [156] of an increase in the amount of Ir atoms with low coordination number in the surface of the catalysts (C_7 sites in Ir(110)-(1x2)).

The data in Figs. 42 and 43 imply that different reaction mechanisms occur on Ir(111) and Ir(110)-(1x2). The dependence of n-butane hydrogenolysis with respect to the partial pressures of the reactants supports the following reaction mechanism on Ir(110)-(1x2) [156]:

$$n-C_4H_{10,g} \quad = \quad C_4H_{8,a} \quad + \quad 2H_a \qquad (32)$$

$$C_4H_{8,a} \quad = \quad 2C_2H_{4,a} \qquad (33)$$

$$C_2H_{4,a} + 2H_a \quad \rightarrow \quad C_2H_{6,g} \qquad (34)$$

The stoichiometry of the C_4H_8 fragment is consistent with a 1,4-diasorbed species or, more specifically a metallacycle pentane that involves the C_7 atoms of the surface [156]. The symmetrical decomposition of this metallacycle is responsible for the very high selectivity found over Ir(110)-(1x2) for ethane production. The formation of a metallacycle pentane is sterically forbidden on the Ir(111) surface [156]. For this close-packed surface (only C_9 atoms, no C_7 atoms, see Fig. 36) a significant repulsion is expected between the α-hydrogens of the metallacycle and the adjacent Ir atoms.

VII.3.2   Rh(111) and Rh(110) Catalysts

The specific turnover frequencies for the production of methane, ethane and propane from n-butane hydrogenolysis on Rh(110) and Rh(111) are plotted in Fig. 44 [165]. For Rh(110), the order of abundance of the products is methane > ethane > propane. The high ethane selectivity seen over Ir(110) [156] is not observed on the Rh(110) surface, presumably because the Rh surface does not exhibit the (1x2) missing-row reconstruction that is stable on Ir(110) surfaces under reaction conditions [165]. This precludes the presence of C_7 sites on Rh(110) preventing the formation of the metallocyclopentane species that is responsible for the high selectivity toward ethane in n-butane hydrogenolysis.

On Rh(110) the apparent activation energy for all three products was 135 ± 6 kJ/mol at temperatures below 500K (see Fig.

44a). Above 500K, the product distribution shifted to reflect more complete hydrogenolysis (i.e. decrease in ethane and propane selectivity). This behavior is qualitatively similar on Rh(111), with the changes in selectivity and "rollover" occurring at a lower temperature (~ 475K). The "rollovers" in Fig. 44 can be ascribed to a decrease in the surface concentration of hydrogen [165].

VII.3.3 Pt(100), Pt(111), Pt(332), Pt(557), Pt(10,8,7) and Pt(13,1,1) Catalysts

The hydrogenolysis of n-butane was investigated on the (100), (111) and (13,1,1) faces of platinum at 573K with P_{H2}/P_{butane}= 10 and P_{total}= 220 Torr [166]. Under reaction conditions the flat (100) and stepped (13,1,1) surfaces contain high concentrations of square (100) microfacets. The initial reaction rates of n-butane hydrogenolysis were very similar on the three surfaces investigated: Pt(111)= 0.0071 C_4H_{10} molec/Pt atom s , Pt(100)= 0.0087 C_4H_{10} molec/Pt atom s, and Pt(13,1,1)= 0.0098 C_4H_{10} molec/Pt atom s . The (111) surface produced a statistical hydrogenolysis distribution (40% methane, 30% ethane and 30% propane) whereas the (100) and (13,1,1) faces displayed much higher selectivities for scission of the internal C-C bond (50-60% ethane production).

Product accumulation curves determined as a function of reaction time for isobutane hydrogenolysis over six different Pt surfaces are compared in Fig. 45 [166]. The hydrogenolysis

reaction displays a significant structure sensitivity. At 573K, the apparent activation energy on Pt(100) (146.5 kJ/mol) was substantially larger than on the kinked Pt(10,8,7) surface (~ 67 kJ/mol) [166]. Over Pt(111), Pt(332), Pt(557) and Pt(10,8,7) hydrogenolysis of isobutane produced mainly methane (55-70%) and propane (25-35%). The (100) and (13,1,1) surfaces yielded more ethane (40-50%) and less methane and propane than the other platinum crystal faces.

VII.4   Neopentane Hydrogenolysis

VII.4.1   Ir(111) and Ir(110)-(1x2) Catalysts

Studies for neopentane hydrogenolysis on Ir(111) and Ir(110)-(1x2) at T=450-600K, P_{H2}= 100 Torr and P_{C5H12}= 1 Torr indicated essentially identical catalytic activities (10^{-4}-10 C_5H_{12} molecules site^{-1} s^{-1}) and activation energies ($E_a \approx$ 151 kJ/mol for T < 500K; $E_a \approx$ 104 KJ/mol for T > 500K) for these surfaces [156]. At T < 500K the major products of the reaction were methane and isobutane, while methane clearly dominated (>60%) at T > 500K . An adsorbed species with C_5H_7 or C_5H_8 stoichiometry was the precursor to the initial C-C bond cleavage [156].

VII.4.2   Pt(111), Pt(100), Pt(10,8,7) and Pt(13,1,1) Catalysts

The hydrogenolysis of neopentane over several faces of platinum was investigated at 573K, P_{H2}= 200 Torr and P_{C5H12}= 20 Torr [166]. The catalytic activity of the surfaces followed the trend: Pt(111) < Pt(100) $\approx$ Pt(13,1,1) < Pt(10,8,7) . Methane and isobutane were the major products. Demethylation represented 75-90% of the reaction over Pt(111) and Pt(10,8,7), but only 65-75% on Pt(100) and Pt(13,1,1). An apparent activation energy of ~ 220 kJ/mol was observed for neopentane hydrogenolysis over Pt(10,8.7) at temperatures in the range between 540 and 590 K [166].

VII.5   N-hexane Hydrogenolysis

VII.5.1   Pt(100), Pt(111), Pt(332), Pt(10,8,7), Pt(13,1,1), Au-Pt(100) and Au-Pt(111) Catalysts

Fig. 46 shows the activity for n-hexane hydrogenolysis of a series of five platinum single crystal surfaces with variable terrace, step and kink structure [167]. The hydrogenolysis rates display little dependence on surface structure, although hydrogenolysis product distributions were influenced markedly by terrace structure [167]. Surfaces with (100) terraces (Pt(100) and Pt(13,1,1), see Fig. 45) displayed a clear preference for scission of internal C-C bonds leading primarily to the formation of ethane, propane and butane. In contrast, surfaces with (111) terraces (Pt(111), Pt(332) and Pt(10,8,7), see Fig. 45) showed a high selectivity for terminal hydrogenolysis. Multiple C-C bond breaking processes were favored at high reaction temperatures

(>600K) and appeared to occur most easily on the (111), (332) and
(10,8,7) platinum surfaces [167]. This phenomenon correlates with
a reduction in the surface concentration of chemisorbed hydrogen
at high temperature. The Pt surfaces that showed larger changes
in selectivity were those with the lower heat of adsorption for
hydrogen (those presenting (111) microfacets) [167].

The hydrogenolysis of n-hexane (P_{H2}/P_{hexane}= 10, P_{total}= 220 Torr
and T= 570K) has been studied on Au-Pt(111) and Au-Pt(100)
surfaces [168,169]. The catalysts were prepared by vapor-
depositing Au onto the (111) or (100) crystal faces of Pt to form
either an epitaxial overlayer or an alloy system. In both cases,
the Au effects on Pt(111) were identical: a large reduction in
the hydrogenolysis activity of the surface with increasing Au
coverage. The corresponding large inhibition of n-hexane
hydrogenolysis over Au-Pt(100) was not observed, indicating a
less severe ensemble size constraints for the reaction on the
more open, fourfold (100) surface [169].

VII.6   N-heptane Hydrogenolysis
VII.6.1   Pt(111), Pt(557), Pt(10,8,7) and Pt(25,10,7) Catalysts

The hydrogenolysis of n-heptane at T=533-603K, P_{H2}= 480 Torr
and $P_{n-C7H16}$= 15 Torr was studied over the flat (111), stepped
(557), and kinked (10,8,7) and (25,10,7) faces of platinum [178].
The hydrogenolysis activity increased in the order: (557) <
(10,8,7) < (111) < (25,10,7), with the Pt(25,10,7) surface being
~ 4.5 times more active than the Pt(557) surface. In general, the

reaction rates decreased with increasing reaction time [178].
This decrease was shown to be the result of the deposition of
irreversibly adsorbed carbonaceous species. The apparent
activation energy for hydrogenolysis on an initially clean
Pt(10,8,7) surface was 58.6 ± 8.5 kJ/mol and on the Pt(111) was
77.9 ± 8.5 kJ/mol [178]. Preoxidation of the single-crystal
catalysts led to an increase in the rate of n-heptane
hydrogenolysis [178].

VII.7   Cyclopropane Hydrogenolysis
VII.7.1   Ni(100) and Ni(111) Surfaces

Fig. 47 shows the results of the reaction of cyclopropane (1
Torr) with hydrogen (100 Torr) over Ni(100) and Ni(111) catalysts
[170]. As seen for supported Ni catalysts, under hydrogen-rich
conditions, the only observed products of the reaction were
methane, ethane and propane [170]. From the data in Fig. 47, we
can conclude that cyclopropane hydrogenolysis to ethane and
methane is a structure-sensitive reaction on Ni surfaces. In
complete analogy with the results for ethane hydrogenolysis (see
above), the activity of the (100) surface is decidedly higher
than that for the (111) surface.

The results for the single crystals are qualitatively
similar to results for supported Ni catalysts [170]. Lower
temperatures tend to produce more simple ring-opening product
(propane), whereas higher temperatures tend to promote complete
C-C bond cleavage, i.e., larger amounts of methane. The apparent

activation energies associated with total hydrogenolysis on Ni(111) and Ni(100), 117.2 and 71.2 kJ/mol respectively [170], are consistent with values typically found for transition metal catalysts (92-126 kJ/mol [171]). Likewise, the corresponding activation energies for the ring-opening reaction over Ni(111) and Ni(100), 58.6 and 62.8 kJ/mol respectively, are very close to those reported for a variety of high-surface area catalysts (46-67 kJ/mol [172-175]).

Fig. 48a shows the effect that progressive sulfiding of a Ni(111) catalysts has on the cyclopropane/hydrogen reaction. The consequences of the presence of S adatoms are threefold: (1) a reduction in the C-C bond breaking ability (i.e. a decrease in ethane and methane production), (2) an increase in the relative propane + propylene yield, and (3) the appearance of significant amounts of ethylene product. Qualitatively the results for the (111) and (100) surfaces are similar in many aspects (see Fig. 48). A notable difference is the absence of ethylene product for the sulfided Ni(100) surface.

VII.7.2 Mo(100) Surface

The catalytic hydrogenolysis of cyclopropane has been investigated over initially clean Mo(100) surfaces and over surfaces chemically modified by adsorbed carbon, oxygen and sulfur [176]. Initially clean Mo(100) surfaces and surfaces covered by 1 ML of atomic carbon or oxygen were active for single hydrogenolysis to propane and double hydrogenolysis to ethane and

methane. A Mo(100) surface with 0.8 ML of sulfur was completely inactive. The reaction was first order in H_2 and zero order in cyclopropane.

The accumulation of ethane at 323, 423 and 523K from an initially clean Mo(100) surface is shown in Fig. 49 [176]. Deactivation is observed at temperatures greater than 373K. Two possible causes of deactivation are carbon deposition and sulfur segregation [176]. After reaction the measured carbon coverage of initially clean Mo surfaces was ~ 0.75 ML. Arrhenius plots for ethane formation on initially clean, C- and O-modified Mo(100) surfaces are reported in Fig. 50 [176]. The activation energy is the same for all the surfaces: 37 ± 4 kJ/mol. However, the activity of initially clean Mo(100) is approximately five times greater than the activity of the modified surfaces. The product distribution was similar for all the active surfaces (ca. 17% CH_4, 17% C_2H_6 and 66% C_3H_8) and independent of temperature [176]. The observed selectivities are in good agreement with data reported for catalysts containing Mo in a low oxidation state [176].

It has been proposed that the active sites of Mo(100) for cyclopropane hydrogenolysis are the open fourfold hollows of the surface [176]. On these sites, it is likely that cyclopropane forms a 1,3-diasorbed C_3H_6 species. This intermediate can be hydrogenated to yield propane, or it can decompose forming hydrocarbon fragments that upon hydrogenation produce ethane and methane [176].

VII.7.3 Pt(s)-[6(111)x(100)] Surface

The hydrogenolysis of cyclopropane at T=350-410K, P_{H2}= 675

Torr and P_{C2H6}= 135 Torr was studied over a platinum stepped

single crystal: Pt(s)-[6(111)x(100)]. This surface consists of

terraces of (111) orientation and 6 atomic rows in width, with

steps of (100) orientation and one atom in height [4]. The rate

~~of propane formation as a function~~ of temperature is summarized

in Fig. 51 . The apparent activation energy calculated from this

plot is 51.1 ± 4.2 kJ/mol [4]. Activation energy values reported

in the literature for this reaction on platinum catalysts range

from 34 to 51 kJ/mol [4]. The hydrogenolysis rates observed on

Pt(s)-[6(111)x(100)] are in reasonable agreement with rates

reported in the literature for alumina supported Pt catalysts

[4].

VII.7.4 Ir(111) and Ir(110)-(1x2) Surfaces

Specific rates for the reaction of cyclopropane with H_2 over

Ir(111) and Ir(110)-(1x2) are shown in Fig. 52, plotted in an

Arrhenius form [177]. The results of this figure indicate a

slightly structure sensitive reaction: the specific activity of

the Ir(110)-(1x2) catalyst is greater than that of the Ir(111)

catalyst, the ratio varying between a factor of 2 and 10 [177].

The rates observed for propane production over Ir(111) agree well

with values found over silica-supported Ir catalysts [177]. On

Ir(111), c-C_3H_6 hydrogenolysis produced methane, ethane,

ethylene, propane and propylene (in Fig. 52 total C_3 product

refers to propane and propylene). In contrast, the only reaction products observed on the Ir(110)-(1x2) surface were methane, ethane and propane. At T < 475K the major product of the reaction was propane, while at T > 500K methane production dominated. For T= 375-450K the apparent activation energy associated with the production of propane (c-C_3H_6 + H_2 → C_3H_8, E_a≈ 38 kJ/mol) was much lower than that for the production of methane and ethane (c-C_3H_6 + 2H_2 → CH_4 + C_2H_6, E_a≈ 104 kJ/mol [177]). These observations can be interpreted [177] by a reaction mechanism involving the relatively facile formation of a metallacycle butane (the step that "opens" the ring), with the rate-limiting step being C-C bond cleavage in this intermediate (i.e., subsequent hydrogenation and desorption are rapid with respect to C-C bond breaking in the metallacycle species).

Fig. 53 illustrates the effects of P_{H2} and P_{c-C2H6} upon the reaction of cyclopropane and hydrogen over Ir(111) at 573K [177]. A dramatic shift in the selectivity is observed for P_{H2}/P_{c-C2H6} <50. Post-reaction surface characterization by AES indicated that the carbon coverage increased from a value of θ_C≈ 0.46 ± 0.1 to values of θ_C≈ 0.8-1.0 ± 0.1 , as P_{H2}/P_{c-C2H6} was reduced below a value of 50 at a temperature of 575K [177]. Fig. 54 compares the changes in selectivity for C_3 and (C_1+C_2) production with the variation in the surface carbon coverage measured after reaction. It has been proposed [177] that the selectivity shifts in Figs. 53 and 54 are a consequence of changes in either the structure or the binding energy of the adsorbed hydrocarbon fragment that

81

precedes the formation of ethane and methane on Ir(111). For Ir(110)-(1x2) the selectivities of c-C_2H_6 hydrogenolysis also showed a strong dependence with the $P_{H2}/P_{c\text{-}C2H6}$ ratio [177]. The onset of the selectivity shifts observed on Ir(111) at $P_{H2}/P_{c\text{-}C2H6} <$ 50 (see Fig. 54) occurred on Ir(110)-(1x2) at $P_{H2}/P_{c\text{-}C2H6} <$ 10.

VII.8 Methylcyclopropane Hydrogenolysis

VII.8.1 Ir(111) and Ir(110)-(1x2) Surfaces

The hydrogenolysis of methylcyclopropane was investigated on Ir(111) and Ir(110)-(1x2) at P_{H2}= 20-500 Torr, $P_{c\text{-}C3H5CH3}$= 0.4-10 Torr and T= 375-700K [177]. On both catalysts the major product of the reaction was n-butane. Other reaction products observed were methane, ethane, propane, isobutane and a mixture of 1- and 2-butenes. The major hydrogenation /isomerization channel over Ir(111) and Ir(110)-(1x2) is given by

$$c\text{-}C_3H_5CH_3 + H_2 \rightarrow n\text{-}C_4H_{10} \qquad (35)$$

whereas the major hydrogenolysis channel is

$$c\text{-}C_3H_5CH_3 + H_2 \rightarrow CH_4 + C_3H_8 \qquad (36)$$

on Ir(111), and

$$c\text{-}C_3H_5CH_3 + H_2 \rightarrow CH_4 + C_2H_6 + C_3H_8 \qquad (37)$$
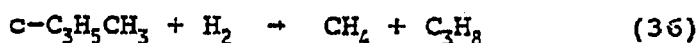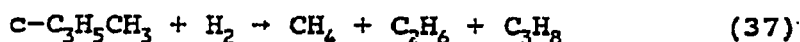
on Ir(110)-(1x2). The absence of ethane in the major hydrogenolysis channel over Ir(111) can be explained purely on a stereochemical basis [177]. The presence of ethane from hydrogenolysis of methylcyclopropane can only be observed by the fragmentation of a metallacycle butane that has been formed by the activation of the C_1-C_2 bond. The methyl group provides a

steric limitation to the activation of the C_1-C_2 bond on a flat Ir(111) surface. On the other hand, a metallacycle butane involving the rupture of the C_1-C_2 bond can be formed with the low-coordination-number C_7 atoms that are present on Ir(110)-(1x2) (see Fig. 36).

VII.9   Methylcyclopentane   Hydrogenolysis

VII.9.1   Pt(100), Pt(111), Pt(332) and Pt(557) Catalysts

The reaction between methylcyclopentane (20 Torr) and hydrogen (600 Torr) was investigated at T= 540-650K over four platinum single crystal surfaces with flat (100) and (111), and stepped (332) and (557) orientations [179]. The main reaction products were 2- and 3-methylpentane; very little n-hexane, cyclopentane or methane was formed. The rate of formation of methylpentanes was found to be nearly two times faster on the (100) surface than on the (111) surface. The presence of steps on the platinum surface had no significant effect on the rates of ring opening since these line defects were quickly covered with carbonaceous deposits [179]. Apparent activation energies were determined for the Pt(111) and Pt(100) surfaces [179], and the following values were determined in kJ/mol: 37-46 for 2- and 3-methylpentane, 59-75 for methane and 105-109 for hydrogenolysis to C_2-C_5 products.

VII.10 Cyclohexane Hydrogenolysis

VII.10.1 Pt(111), Pt(557), Pt(25,10,7) and Pt(10,8,7) Catalysts

Fig. 55 shows results for cyclohexane hydrogenolysis on the flat (111), stepped (557), and kinked (25,10,7) and (10,8,7) faces of platinum [180]. The hydrogenolysis rates were highest on Pt(111). In general, the reaction rates decreased with increasing reaction time due to the irreversible adsorption of a tightly bound carbonaceous deposit [180]. Fig. 56 illustrates the dependence of initial rates on H_2 pressure over the Pt(111) and Pt(10,8,7) surfaces [180]. Hydrogenolysis leading to n-hexane is positive order in hydrogen on both surfaces at low hydrogen pressure, but becomes negative order at pressures greater than 400 Torr. Light alkane production is slightly negative order in hydrogen pressure.

VII.10.2 Ru(001) and Cu/Ru(001) Catalysts

The hydrogenolysis of cyclohexane was investigated on Ru(001) at P_{H2}= 20-100 Torr, $P_{c-C6H12}$= 1-4 Torr and T= 570-650K [181]. In all the cases investigated, initially clean Ru(001) showed the highest activity for producing C_1-C_6 hydrocarbons. The hydrogenolysis activity of the catalyst decreased with time up to a constant (steady-state) value. At this point the Ru(001) surface was covered by ~ 1 ML of carbon and the major product of the $c-C_6H_{12}+H_2$ reaction was benzene [181]. The decrease in hydrogenolysis rates with carbon coverage indicates, at the very least, that C-C bond scission , generally recognized as the rate-

84

determining step in hydrogenolysis reactions, is slower in the presence of carbon than on the clean Ru(001) surface [181]. From the data in Fig. 57, it appears that cyclohexane hydrogenolysis on Ru(001) is negative order in cyclohexane and positive order in hydrogen partial pressures [181]. This type of dependence is believed to reflect the response of the surface carbon level to changes in cyclohexane and hydrogen pressures (positive w.r.t. cyclohexane and sharply negative w.r.t. hydrogen) [181].

Studies for Cu/Ru(001) show a reduction in the rate of cyclohexane hydrogenolysis with increasing Cu coverage [181]. Several mechanisms have been proposed which may account for the altered properties of the Ru(001) catalyst upon addition of Cu [181]. In the simplest one, Cu may be acting much like C in that the intermediate preceding hydrogenolysis is stabilized toward C-C bond scission.

VIII.   ISOMERIZATION AND CYCLIZATION OF ALKANES

Catalytic reforming is one of the basic petroleum refining processes, yielding a large variety of liquid fuels [10,11,134]. In reforming, paraffins are reconstructed without changing their carbon numbers. The reactions, which include isomerization of n-alkanes to isoalkanes and dehydrocyclization of n-alkanes to alicyclics and aromatics, lead to a marked improvement in fuel quality as measured by the octane number [11,134]. Typical industrial reforming catalysts are generated by dispersing crystallites of Pt or Pt alloys on alumina. The isomerization of

light alkanes on Pt single-crystal surfaces has been intensively
investigated in recent years from the viewpoint of catalysis
[166-169,178,182-184]. It has become evident that the catalytic
chemistry of the platinum-hydrocarbon interface is interesting,
unique and important [183].

VIII.1 Butane Isomerization

VIII.1.1   Pt(111), Pt(100), Pt(332), Pt(557), Pt(13,1,1) and Pt(10,8,7) Catalysts

The interaction between H_2 (200 Torr) and n-butane (20 Torr)
was investigated on the (100), (111) and (13,1,1) faces of
platinum at 573K [166]. Isomerization, dehydrogenation and·
hydrogenolysis of n-butane were observed. The reaction rates for
the processes followed the order: dehydrogenation > isomerization
> hydrogenolysis. The fractional isomerization selectivities
($S_{isom} = R_{isom} / (R_{isom} + R_{hydrogenolysis})$) varied from 0.65 on Pt(111) to ~
0.8 on Pt(100) and Pt(13,1,1). The isomerization reaction
displayed substantial structure sensitivity: the catalytic
activities of the (100) and (13,1,1) platinum surfaces were at
least three times higher than that for Pt(111) [166]. AES showed
a carbon coverage of 1.7-2.7 ML on the Pt surfaces after a 90-150
min reaction time [166].

Product accumulation curves for isobutane isomerization over
the flat (100) and (111), stepped (332), (557) and (13,1,1), and
kinked (10,8,7) faces of platinum are shown in Fig. 58 [166].
Under the experimental conditions of this figure, isobutane

dehydrogenation produced equilibrium concentrations of isobutene within minutes over all six platinum surfaces [166]. The initial rate of dehydrogenation was at least 2-6 times faster than those for isomerization and hydrogenolysis. In general, the fractional isomerization selectivities (S_{isom}) were larger than 0.85 . In Fig. 58 the order of activity for isomerization follows the sequence Pt(100) $\approx$ Pt(13,1,1) > Pt(557) > Pt(10,8,7) $\approx$ Pt(332) > Pt(111), with the difference in initial rates between the least- and most-active crystal face being approximately a factor of 6. High concentrations of (100) microfacets were required for high catalytic activity in butane isomerization. Arrhenius plots for isobutane isomerization on the (100) and (10,8,7) platinum surfaces are compared in Fig. 59 [166]. The isomerization activity of Pt(100) displayed a maximum at about 600K and then decreased with increasing temperature.

VIII.2   Neopentane Isomerization

VIII.2.1   Pt(100), Pt(111), Pt(13,1,1) and Pt(10,8,7) Catalysts

Fig. 60 displays the activity of four different faces of Pt for neopentane isomerization [166]. In contrast to the C_4 alkane reactions, surface structure had only a small influence on the initial rates of neopentane isomerization. The fractional isomerization selectivities (S_{isom}) varied between 0.85 and 0.90 . The selectivity in isomerization for n-pentane production displayed notable structure sensitivity [166]. While the Pt(111)

87

and Pt(10,8,7) catalysts yielded only 2-3% n-pentane in isomerization, the (100) and (13,1,1) surfaces produced 12-14% n-pentane. For T= 540-570K the initial rates of neopentane isomerization displayed an apparent activation energy of 217.6 kJ/mol on Pt(10,8,7) [166]. Above 580K the initial reaction rates were insensitive to changes of temperature [166]. The rates of isomerization decreased with time due to the deposition of carbon on the Pt catalysts. The rate of deactivation of the surfaces increased with increasing reaction temperature. Deactivation was accompanied by the deposition of about one monolayer of strongly chemisorbed carbonaceous species [166].

VIII.3 Methylpentane Isomerization and Cyclization
VIII.3.1 Pt(111), Pt(119), Pt(311) and Pt(557) Catalysts

The isomerization of 2- and 3-methylpentane was investigated over Pt(111), Pt(119), Pt(311) and Pt(557) at P_{H2}= 755 Torr, P_{HC}= 5 Torr and T= 623K [182,184]. On all the surfaces, the major products of 2-methylpentane isomerization were methylcyclopentane and 3-methylpentane, with minor amounts of n-hexane and benzene. Similar results were observed for polycrystalline Pt and alumina supported Pt catalysts [182]. Isomerization of 3-methylpentane on Pt(557) yielded mainly methylcyclopentane and 2-methylpentane with no benzene in the products. For the examined platinum catalysts, the flat (111) surface showed the highest activity for hydrogenolysis and the lowest for isomerization.

VIII.4   N-hexane Isomerization and Cyclization

VIII.4.1   Pt(100), Pt(111), Pt(332), Pt(13,1,1), Pt(10,8,7), Au-Pt(100) and Au-Pt(111) Catalysts

The reaction of H_2 (200 Torr) and n-hexane (20 Torr) was studied at 573K on flat ((100) and (111)), stepped ((332) and (13,1,1)) and kinked ((10,8,7)) surfaces of Pt [167]. Only the aromatization reaction displayed significant structure sensitivity that was characterized by about a factor of 4 difference in initial rates between the most active (10,8,7) and least active (100) platinum surfaces [167]. In general, the selectivity for cyclization (benzene + methylcyclopentane production) varied between 50 and 60%, while that for isomerization (2- and 3-methylpentane production) was in the range between 20 and 30% . Skeletal rearrangement was dominated by cyclic mechanisms involving both 1,5- and 1,6-ring closure [167]. Polymerization of the adsorbed species competed with skeletal rearrangement and lead to the growth of a disordered carbonaceous deposit (one or more monolayers) on the platinum surfaces [167]. The primary role of this deposit was that of a nonselective poison.

Arrhenius plots for n-hexane isomerization, C_5-cyclization and aromatization catalyzed over five platinum surfaces are shown in Figs. 61 and 62 [167]. Surfaces with a high concentration of (111) microfacets (Pt(10,8,7), Pt(332) and Pt(111), see Fig. 45) were always more active in aromatization than those rich in (100) terraces (Pt(13,1,1) and Pt(100), see Fig. 45). All other

reactions displayed little structure sensitivity at all reaction temperatures.

The catalytic conversion of n-hexane was studied over Au-Pt(100) and Au-Pt(111) alloys [168,169]. In Fig. 63 the initial rates (initial rates per surface atom, i.e., gold and platinum) of isomerization, C_5 cyclization, aromatization and hydrogenolysis are shown as a function of surface alloy composition. The data in the figure show the structure sensitivity of alloy catalysis for hydrocarbon conversion [169]. The effects of Au concentration upon the formation of 2- and 3-methylpentane and the rate of hydrogenolysis are different for each surface. In particular, the Au-Pt(111) system shows an increase in the rate of isomerization that is not observed on Au-Pt(100). The total activity of the Au-Pt(100) alloy decreased linearly with increasing surface atom fraction of gold [169]. In contrast, the Au-Pt(111) alloy showed an enhancement in the total activity as the surface atom fraction of gold was increased from 0 to 0.4, and then fell off with further increase in the surface atom fraction of gold [169].

The results of the Au-Pt(111) surface can be interpreted in terms of differences in ensemble requirements [168,169]. It appears that hydrogenolysis and aromatization require large ensembles of platinum atoms. The dilution of the Pt surface with Au reduces the number of these large ensembles, inhibiting these reactions. The blocking of these reaction pathways provides more surface species for reactions that require only small ensembles

of Pt atoms. The result is an enhancement in the rate of
isomerization per Pt atom with increasing surface atom fraction
of Au [168,169]. For Au-Pt(100), there is no enhancement in the
rate of n-hexane isomerization. The reaction mechanism that
occurs for the (111) alloy surfaces was not available on the
(100) alloy surfaces, probably due to differences in the
morphology and/or in the electronic properties of these
bimetallic surfaces [168,169].

VIII.5 N-heptane Cyclization
VIII.5.1 Pt(111), Pt(557), Pt(10,8,7) and Pt(25,10,7) Catalysts

Fig. 64 shows toluene accumulation curves from n-heptane
cyclization on four different faces of platinum [178]. The
initial rate of toluene production increased in the order (111) $\approx$
(25,10,7) < (557) $\approx$ (10,8,7). Fig. 65 compares the initial rates
measured for toluene production and n-heptane hydrogenolysis
[178]. The selectivity of toluene production versus
hydrogenolysis increased by an order of magnitude in the sequence
(25,10,7) < (111) < (10,8,7) < (557). The apparent activation
energy for toluene formation was 126.6 $\pm$ 16.74 kJ/mol on the
clean Pt(10,8,7) surface and 140.6 $\pm$ 8.4 kJ/mol on the clean
Pt(111) surface [178]. In general, the reaction rates decreased
with increasing reaction time. This decrease was shown to be the
result of the deposition of irreversibly adsorbed carbonaceous
species [178].

VIII.6 Summary

The results discussed above show significant differences in isomerization activity for platinum single-crystal surfaces with different atomic structures. Fig. 66 summarizes initial rates as a function of crystallographic orientation for the isomerization of n-butane, isobutane, neopentane and n-hexane at 573K [166,167]. The butanes display the maximum variation in reaction rate with surface structure. High concentrations of (100) terraces were required for high catalytic activity in butane isomerization [166]. The effect of steps and kinks was to increase the isomerization rates, although this effect was small as compared to the changes introduced by terrace structure. Neopentane and n-hexane isomerization display little dependence on platinum surface structure. The absence of structure sensitivity in the isomerization of n-hexane has been explained in terms of a reaction mechanism that is dominated by C_5 cyclic intermediates [166,167]. These intermediates cannot be formed during the isomerization of light alkanes.

The results in Fig. 66 indicate that the rate of isomerization depends markedly upon the structure of the reacting hydrocarbon [166]. The order of isomerization activities follows the sequence neopentane ≥ isobutane > n-butane > n-hexane . This trend suggests that isomerization rates increase with increasing degree of substitution and decreasing molecular weight [166].

The isomerization activity of carbon-covered platinum surfaces appears to be lower than that of clean platinum.

Hydrocarbon overlayers that are pre-adsorbed on Pt act as poisons [183]. During actual catalytic conditions more than 50% of the catalyst surface was covered by carbonaceous deposits within the first few minutes of reaction [183,185]. These residues grew continuously passivating the metal and inhibiting further hydrocarbon conversion. A significant difference in deactivation behavior between the light-alkane and n-hexane reaction studies was in the amount of carbon deposited [166,185]. At any given temperature, less carbon was deposited on the Pt surfaces during light-alkane isomerization. In these cases, the defect sites (steps and kinks) were not readily covered by hydrocarbon residues and were therefore available for catalysis. The presence of kinks and steps had an appreciable influence in the rate of isomerization of isobutane on Pt surfaces [185]. The same effect was not observed for methylcyclopentane or n-hexane conversion, because these heavier alkanes deposited carbonaceous fragments at the surface irregularities and passivated them within the first minutes of reaction, so the catalysis occurred only on the terraces of the Pt surfaces [185].

IX. HYDROGENATION OF OLEFINS

A great variety of hydrogenation reactions involving olefins are carried out industrially. These range from large-scale continuous catalytic operations in petroleum refineries to small-scale batch operations in the pharmaceutical and fine chemical industry [10,11]. The addition of hydrogen across a C=C bond is

one of the easiest and most studied of metal catalyzed reactions [11,183]. The most active metallic catalysts are those in group VIII . Studies using single-crystal catalysts have been primarily focused on the hydrogenation of ethylene and light olefins (C_3-C_6) [177,186-192].

IX.1. Ethylene Hydrogenation

IX.1.1. Pt(111) Surface

The hydrogenation of ethylene to ethane using both hydrogen and deuterium was investigated on the flat Pt(111) surface at temperatures between 300 and 373K [186]. Arrhenius plots are shown in Fig. 67, yielding an apparent activation energy of 45.2 ± 0.5 kJ/mol . This value agrees well with results for supported Pt catalysts that show activation energies in the range between 38 and 45 kJ/mol [186]. On Pt(111), ethylene hydrogenation exhibits a normal isotope effect: the reaction with hydrogen is about 1.3 times faster than with deuterium [186]. Reaction orders of 1.31 ± 0.05 with respect to hydrogen (or deuterium) and -0.60 ± 0.5 with respect to ethylene were observed. All these kinetic data compares favorably with results reported for high surface area Pt catalysts [186].

Fig. 68 shows a typical product distribution for the reaction of ethylene and D_2 [186]. The deuterium atom distribution in the reaction products peaks at 1-2 deuterium atoms per ethane molecule produced, similar to what has been reported for supported Pt catalysts [186].

AES spectra taken after reaction conditions revealed a metal surface covered by hydrocarbon species [186]. No reaction self-poisoning was detected during the hydrogenation experiments. Furthermore, when reactions were started on surfaces covered by hydrocarbon fragments, either by retaining the carbonaceous deposits from previous reactions or by predosing the surface to ethylene under UHV conditions, the rates were identical to those seen when starting with a clean Pt(111) surface [186]. Evidence from LEED and TDS suggests that the carbonaceous species found on the catalyst surface after reaction are, in fact, ethylidyne moieties, as obtained by dosing ethylene onto a clean Pt(111) surface in UHV [186]. The hydrogenation rate of the ethylidyne adlayer was much slower than the rates of ethylene hydrogenation [186]. It has been proposed that ethylene hydrogenation does not take place on the clean metallic surface but rather on top of a layer of carbonaceous fragments composed mainly by ethylidyne adsorbates [186]. According to this mechanism H_2 dissociates on the metal, while ethylene is weakly adsorbed on top of the carbonaceous deposits. The main role of the ethylidyne species is to transfer H atoms from the metal surface into the adsorbed ethylene molecules [186]:

$$H_{2,g} = 2H_a \tag{38}$$

$$Pt_3{\equiv}CCH_{3,a} + H_a \rightarrow Pt_n{=}CHCH_{3,a} \tag{39}$$

$$2Pt_n{=}CHCH_{3,a} + C_2H_{4,a} \rightarrow 2Pt_3{\equiv}CCH_{3,a} + C_2H_{6,g} \tag{40}$$

95
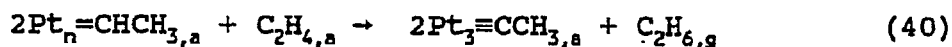
The ability of ethylidyne to exchange hydrogen (or deuterium) atoms with Pt(111) surfaces covered with hydrogen (or deuterium) is well known [186]. The fact that ethylene hydrogenation over Pt(111) is very similar to that on supported Pt catalysts is a consequence of the presence of the ethylidyne adlayer, which masks the surface structure making the reaction surface insensitive [186].

IX.1.2   Ni(100), Ni(110) and Ni(111) Surfaces

Ethylene hydrogenation was performed over the three low-Miller-index faces of nickel, (100), (110) and (111), at 298K under a total pressure of 50 Torr with H_2/C_2H_4 ratios of 10 and 100 [192]. The reaction rate was first order in H_2 pressure and independent of ethylene pressure. At $P_{H2}/P_{C2H4} = 10$, the measured steady-state rates were respectively 0.35 and 0.10 x 10^{19} molecules h^{-1} cm^{-2} for the (111) and (110) faces. On the (100) face practically no reaction was observed under the same conditions. The trend in catalytic activity of the single-crystal surfaces, (100) << (110) < (111), agrees well with results that show a higher catalytic activity for Ni crystallites with (111) orientation than for randomly oriented crystallites [192].

Post-reaction surface analysis with AES showed the presence of carbon on the Ni single-crystal catalysts [192]. C_2H_4 is dissociatively adsorbed on the (100) face forming acetylenic residues, which completely cover the surface and are not displaced when in contact of hydrogen. Consequently, Ni(100) is

96

practically inactive for ethylene hydrogenation. Over the (111)

face, the acetylenic residues are rearranged on the surface in a

way that leaves free Ni regions in which the catalytic

hydrogenation takes place [192].

Effective poisoning of catalytic activity at sulfur

coverages of less than 0.15 ML has been observed for ethylene

hydrogenation on nickel [151]. Electronic effects, rather than

ensemble requirements, dominate the catalytic poisoning mechanism

[151].

IX.2   Propylene Hydrogenation

IX.2.1   Ir(111) and Ir(110)-(1x2) Surfaces

Steady-state rates of the reaction of propylene with

hydrogen on the Ir(111) and Ir(110)-(1x2) surfaces are shown in

Fig. 69, plotted in Arrhenius form [177]. Two reaction channels

were observed: hydrogenation to propane (E_a= -0.8 kJ/mol on

Ir(111) and -15.1 kJ/mol on Ir(110)-(1x2); T=450-600K) and

hydrogenolysis to methane and a mixture of ethane and ethylene

(E_a= 99.6 kJ/mol on Ir(111) and 110.1 on Ir(110)-(1x2); T= 400-

500K). On both Ir surfaces the major reaction product was

propane, with Ir(110)-(1x2) showing a greater activity for

hydrogenation. Measurements of the adsorption and desorption

kinetics of hydrogen on the clean (111) and (110)-(1x2) surfaces

show the presence of a higher binding energy adstate on the

(110)-(1x2) surface [177,193]. Thus, it might be expected that

the hydrogen adatom concentration will be greater on the Ir(110)-

(1x2) surface during reaction conditions, and this could explain the greater rate of hydrogenation seen on the Ir(110)-(1x2) catalyst [177].

AES spectra acquired after the hydrogenation reaction revealed a carbonaceous residue on the surface of the Ir catalysts [177]. The coverage of carbon varied between 0.4 (T ~ 400K) and 1.0 ML (T ~ 600K). The departure from Arrhenius behavior seen in Fig. 69 for propylene hydrogenolysis at ~ 480K was associated with a large increase in the coverage of the carbonaceous residue and a reduction in the coverage of hydrogen adatoms [177]. Fig. 70 illustrates the dramatic effects of the P_{H2}/P_{C3H6} ratio upon the coverage of the carbonaceous residue and the selectivity of the $C_3H_6 + H_2$ reaction at a temperature of 575K [177]. Similar experiments carried out at 450K showed an essentially constant value of $\theta_C \approx 0.5$, with a rate for propane production 10-100 times larger than those for production of methane, ethane and ethylene [177].

IX.3   1,3-Butadiene Hydrogenation

IX.3.1   Pt(100), Pt(110), Pt(111) and Ni$_{0.5}$Pt$_{0.5}$(111) Surfaces

The hydrogenation of 1,3-butadiene was investigated over the (100), (110) and (111) faces of platinum at T= 300-550K, P_{H2}= 100-500 Torr and P_{C4H6}= 5-30 Torr [187-189]. Fig. 71 shows a typical product distribution for butadiene hydrogenation on Pt(111) as a function of reaction time. In all the cases examined, butane and 1-butene were the major initial products,

with minor formation of 2-cis- and 2-trans-butene. Fig. 72 shows initial rates of butadiene consumption on Pt(111) and Pt(100) as a function of inverse temperature. At 330 < T < 480K, the apparent activation energies were: 138 kJ/mol on Pt(100) [188], 164 kJ/mol on Pt(110) [187] and 159 kJ/mol on Pt(111) [189]. The initial turnover numbers increased with the roughness of the surface (111) < (100) < (110) with a ratio of 1 to 4 [189].

Auger spectra taken after reaction conditions showed large amounts of carbonaceous deposits on the surface of the Pt catalysts [188,189]. After any reaction at temperatures below 480K θ_c varied between 1 and 1.5 carbon atoms per platinum atom. At this conditions the carbonaceous adlayers were probably formed by butadiene and C_4H_7 entities which directly participated in the reaction [189]. Butadiene is stable under vacuum without loss of hydrogen until 390K, it appears that under an excess of hydrogen and at temperatures below 480K, the molecules do not dehydrogenate on the Pt surfaces [189]. Above 480K, a continuous decrease in the rate of hydrogenation was observed when the temperature was increased (see Fig. 72). This correlated with an increase in the carbon coverage measured after reaction: 2.5 to 3 ML or even more [189]. This deactivation phenomenon was probably the result of an irreversible decomposition of butadiene.

The order of the hydrogenation reaction with respect to 1,3-butadiene was zero on all the surfaces, while the order in hydrogen pressure varied from 0.5 for Pt(100) to 1 for Pt(110) and Pt(111) [189]. On Pt(100) and Pt(111), the selectivity did

not depend on P_{H2} but changed considerably when P_{C4H6} varied [188,189].

The following reaction scheme has been proposed for the hydrogenation of 1,3-butadiene on Pt surfaces [187,188]:

$$H_{2,g} = 2H_a \qquad (41)$$

$$C_4H_{6,g} = C_4H_{6,a} \qquad (42)$$

$$C_4H_{6,a} + H_a = C_4H_{7,a} \qquad (43)$$

$$C_4H_{7,a} + H_a \rightarrow C_4H_{8,a} \qquad (44)$$

$$C_4H_{8,a} \rightarrow C_4H_{8,g} \qquad (45)$$

$$C_4H_{8,a} + H_2 \rightarrow C_4H_{10,g} \qquad (46)$$
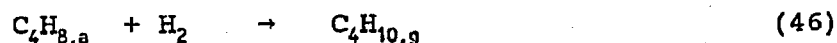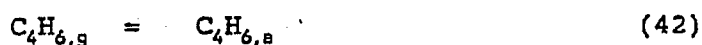
The rate-determining step is probably reaction (44), which corresponds to hydrogenation of the C_4H_7 intermediate. This intermediate exists in two different forms: one leading to 1-butene; the other to 2-butenes (cis and trans). 1-butene can either desorb or be hydrogenated into butane [188,189].

Sulfur adatoms poison the hydrogenation of 1,3-butadiene on Pt(100) [188], Pt(110) [187] and Pt(111) [189]. Fig. 73 displays typical deactivation curves. At high coverage, $\theta_s = 0.5$, the residual activity could be due to defects in the surface or in the S adlayer. The electronic effect usually observed in sulfur poisoning does not exist for butadiene hydrogenation on Pt surfaces [187]. For $\theta_s = 0.2-0.4$, sulfur adatoms did not change the apparent activation energy of the reaction [187-189]. On Pt(100) [188] and Pt(111) [189], sulfur preferentially poisons

100

the sites of 1-butene hydrogenation into butane, decreasing the selectivity toward butane production. For the sulfur modified surfaces butadiene hydrogenation was first order in H_2 partial pressure [188,189].

The hydrogenation of 1,3-butadiene was examined over the (111) face of a $Pt_{0.5}Ni_{0.5}$ alloy [191]. Although the bulk concentration of the alloy was 50 at.% in each component, the surface was largely enriched with platinum. On the $Pt_{0.5}Ni_{0.5}$(111) sample a quasi-complete platinum surface layer (less than 2-4 at.% nickel) was present. This platinum outer layer showed novel catalytic properties with respect to pure Pt [191]. Fig. 74 compares results for 1,3-butadiene hydrogenation on Pt(111) and $Pt_{0.5}Ni_{0.5}$(111). The main features are a higher activity and a better selectivity toward butenes on the alloy sample as compared to pure platinum. The initial activity, measured from the decrease of the butadiene partial pressure, is about 3-4 times larger on the Pt-Ni catalyst.

The different behavior of the alloy sample with respect to pure platinum seems surprising, since on the alloy sample an almost complete platinum outer layer is formed. However, either the Ni atoms in the sublayers may influence the surface metallic atoms or the underlying metal can cause an epitaxial strain in the outer layer, which modifies the physical and chemical properties of the platinum surface atoms [191]. The observation of a strongly contrasted (1x1) LEED pattern suggests that the surface atoms of the alloy are in registry with the bulk lattice,

which is contracted by 4.3% for the alloy with respect to pure
platinum [191].

IX.4   Cyclohexene Hydrogenation

IX.4.1   Pt(223) Surface

Product accumulation curves for the hydrogenation of
cyclohexene on Pt(223) are shown in Fig. 75 [190]. The atomic
structure of the catalyst consists of terraces of (111)
orientation that are five atoms wide, separated by steps of (100)
orientation and one atom in height. At temperatures below ~ 370K,
self-poisoning did not occur and a large fraction of the adsorbed
species that accumulated on the surface was reversibly desorbed
at ~ 390K as molecular benzene. At temperatures higher than 400K,
self-poisoning became rapid and largely irreversible with the
formation of extensively dissociated species with multiple metal-
carbon bonds [190]. This strongly chemisorbed overlayer
decomposed on further heating under vacuum with the evolution of
hydrogen and only minor traces of benzene [190].

The turnover frequencies and reaction probabilities at 423K
for the hydrogenation and dehydrogenation of cyclohexene in
excess hydrogen are summarized in Fig. 76 [190]. The Pt(223)
crystal predominantly produces benzene at low pressures (~10^{-7}
Torr) and cyclohexane at high pressures (~10^2 Torr). The
catalytic activity observed at low pressures is characteristic of
a clean metal surface. At high pressures the initially clean
surface rapidly becomes covered with near a monolayer of

reversibly and irreversibly chemisorbed species. The catalytic behavior is then characteristic of an extensively precovered Pt surface [190].

In Fig. 77 the initial turnover frequencies obtained for the hydrogenation of cyclohexene on Pt(223) as a function of temperature are compared with those observed on supported Pt catalysts [190,194]. The two sets of data agree well, supporting the view that the reaction at high pressures is structure insensitive [190,194]. The apparent activation energy is 20.9 ± 2 kJ/mol on the Pt(223) surface.

X. CYCLOHEXANE DEHYDROGENATION

The aromatization of cyclohexane and alkylcyclohexanes is an important reaction in petroleum refining processes [134]. The dehydrogenation of cyclohexane has been extensively studied as a model reforming reaction [183]. In industrial bifunctional catalysts aromatization of cyclohexane occurs almost exclusively on the metal component [134]. At temperatures between 460 and 590K, platinum is more active than palladium, which appears to be more active than osmium, ruthenium, and nickel in decreasing order of activity (Pt>Pd>Os≥Ru≥Ni) [183]. Continuous deactivation is usually observed due to the formation of a carbonaceous layer on the surface of the catalyst [183]. This layer is formed by reversible adsorbed benzene and by strongly (sometimes irreversibly) chemisorbed carbon deposits.

X.1   Kinetics on Pt Surfaces

The adsorption and dehydrogenation of cyclohexane on Pt(111)
have been extensively studied [195-202]. A sticking coefficient
of near unity was found for $c-C_6H_{12}$ on clean Pt(111) at 100K
[201b]. The heat of chemisorption of the molecule is ~58 kJ/mol
[201]. At ~235K a fraction of the adsorbed $c-C_6H_{12}$ molecules
desorb, whereas the rest begin to dehydrogenate and finally form
benzene by 350K [201,202].

The interaction between hydrogen (100 Torr) and cyclohexane
(15 Torr) was studied on the flat (111), stepped (557), and
kinked (25,10,7) and (10,8,7) faces of platinum [180]. Benzene,
cyclohexane, n-hexane and alkane fragments with carbon number
less than 6 were observed as reaction products. Typical results
obtained with the (10,8,7) surface depicted in Fig. 78,
illustrate the selectivity and deactivation behavior of the four
types of reaction products. Over all the investigated surfaces,
the major dehydrogenation product was benzene [180]. Fig. 79
shows the production of cyclohexene and benzene as a function of
surface structure. The initial rate of benzene production
increased in the order (111) < (557) < (10,8,7) < (25,10,7). In
Fig. 79 the decrease of the dehydrogenation rates was due to
reversible product inhibition by benzene, as well as the
irreversible adsorption of tightly bound carbonaceous deposits
[180]. Product poisoning was found to be structure sensitive,
increasing in the sequence (25,10,7) < (10,8,7) < (557) < (111).

There was a clear correlation between the activity of the surfaces and their sensitivity to product poisoning [180].

The apparent activation energy associated with the initial rate of benzene production was 71.2 ± 8.4 kJ/mol on Pt(111) and Pt(10,8,7) [180]. Dehydrogenation to benzene was approximately first order in cyclohexane pressure [180]. Fig. 56 illustrates the dependence of the initial rates of dehydrogenation and hydrogenolysis on hydrogen pressure over the (111) and (10,8,7) surfaces [180]. On both surfaces, at hydrogen pressures less than 400 Torr, benzene production is positive order in hydrogen. Above 400 Torr the reaction becomes zero order in hydrogen pressure on the (10,8,7) surface, but remains positive order up to at least 745 Torr on the (111) surface.

The dehydrogenation of cyclohexane ($P_{c-C6H12}$= 15 Torr, P_{H2}= 99.75 Torr, T= 573K) has been studied over Au-Pt(111) surfaces prepared by vapor-depositing Au onto the (111) face of Pt to form either an epitaxial overlayer or an alloy system [203]. Cyclohexane was converted into benzene, cyclohexene, and very small amounts of n-hexane and smaller hydrocarbons. The latter two classes of reactions were several orders of magnitude slower than dehydrogenation. The influence of Au on the amount of benzene and cyclohexene formed in 123 min reaction time is shown in Fig. 80. There is an enhancement of the benzene production by gold, which reaches a maximum at a surface gold content of about 50% . The enhancement was observed with both the epitaxial and the alloy surfaces, although it was generally larger with the

surface alloys. For cyclohexene production the maximum

enhancement was found at a surface Au concentration of about 90

atom %, which differs considerably from the composition that gave

maximum benzene production. The catalytic activity that is

observed at high Au coverages is due to contributions from the

crystal edges and imperfections that are not covered by gold

[203].

Au influences cyclohexane dehydrogenation by restricting the

number of Pt atoms available for interaction with adsorbed

benzene [203]. When Pt(111) is alloyed with small amounts of Au,

deep dehydrogenation of benzene no longer takes place and the

product poisoning is reduced. The resulting activity increase is

larger than the reduction of the Pt surface area. At an

intermediate gold surface concentration, the activity reaches a

maximum and declines thereafter as the ensembles of Pt atoms

become too small to catalyze cyclohexane dehydrogenation down to

benzene [203]. At this point, the cyclohexene-like intermediate

that is formed during the dehydrogenation of cyclohexane is no

longer quantitatively converted to benzene but it desorbs as

cyclohexene. Consequently, the maximum of cyclohexene production

is reached at higher gold concentrations than that of benzene

formation [203].

X.2 Kinetics on Ru Surfaces

Fig. 81 shows rates of cyclohexane dehydrogenation and

hydrogenolysis on Ru(001) as a function of reaction time and

carbon coverage present on the catalyst surface after reaction [181]. The rate of benzene production over initially clean Ru(001) was quite low but rose with time to reach a constant value when the surface was saturated with carbon. During the induction time, the formation of lower carbon number alkanes from the hydrogenolysis of cyclohexane was much higher than the rates obtained at steady state. The carbon-modified Ru(001) surface likely stabilizes cyclohexane (and possibly other intermediates leading to the product benzene) with respect to carbon-carbon bond scission [181].

Specific rates of cyclohexane dehydrogenation to benzene obtained under steady-state reaction conditions are plotted in Arrhenius form in Fig. 82a. The apparent activation energy measured, - 75 kJ/mol, is very similar to values of 63-88 kJ/mol obtained on Pt single-crystal and supported catalyst studies [181]. The response of the reaction to changes in the partial pressure of the reactants is shown in Fig. 82b. The rate of benzene formation is zero order in cyclohexane pressure and approximately first order in hydrogen pressure, in good agreement with results on supported catalysts [181].

Fig. 83 shows the effect of addition of Cu to Ru(001) upon the rate of cyclohexane dehydrogenation [181]. The overall rate of the reaction is seen to increase by almost an order of magnitude at a Cu coverage of 0.75 ML . Above this coverage, the rate falls to an activity approximately equal to that of Cu-free Ru(001). The observed non-zero rates at the higher Cu coverages

are believed to be caused by three-dimensional clustering of the Cu overlayers [181]. The rate enhancement observed for submonolayer Cu deposits may be related to an enhanced activity of the strained Cu film for this reaction due to its altered geometric and electronic properties [181]. Alternatively, a mechanism whereby the two metals cooperatively catalyze different steps of the reaction may account for the activity promotion [181]. Dissociation of H_2 on bulk Cu is difficult due to kinetic constraints. In the combined Cu/Ru(001) system, Ru may function as an atomic hydrogen source/sink via spillover to/from neighboring Cu [181]. In addition, Cu may serve to weaken the chemisorption bond of benzene, limiting self-poisoning by the adsorbed product [181].

X.3 Kinetics on W Surfaces

The dehydrogenation of cyclohexane to benzene was studied over W(110) at P_{H2}= 100 Torr, $P_{c-C6H12}$= 1 Torr and T= 630K [204]. A turnover frequency of 0.005 benzene molecules $site^{-1}$ s^{-1} was observed. The dehydrogenation activity of the W(110) surface was increased by adsorbing SiO_x species [204]. A W(110) catalyst covered by a monolayer of silicon oxidized 35% showed a turnover frequency of 0.019 benzene molecules $site^{-1}$ s^{-1} , i.e. ~ 4 times the activity of clean W(110).

XI. CYCLOTRIMERIZATION OF ACETYLENE

XI.1 Kinetics on Pd Surfaces

The conversion of acetylene to benzene on Pd surfaces is a reaction which proceeds readily at conditions ranging from UHV (10^{-9} Torr) to atmospheric pressures (10^3 Torr) [205-209]. The cyclization of acetylene to benzene occurs on Pd(111), Pd(100) and Pd(110) at temperatures below 250K [205]. The results of Fig. 84 show a structure sensitive reaction. In UHV the (111) face is the most active followed by the (110) and then the (100) surface [205]. At high pressure the (111) and (100) surfaces have equal catalytic activity whereas the (110) face is one-fourth as active [205].

At high pressure conditions, an apparent activation energy of 8.4 kJ/mol was observed for the trimerization reaction over Pd(110), Pd(111) and Pd(100) (see Fig. 85a). The reaction rate was first order in acetylene partial pressure (see Fig. 85b). Analysis of the catalysts by AES after reaction showed partially carbon-covered surfaces [205]. It appears that acetylene cyclization takes place on top of the bare metal sites. The irreversibly bound carbon limits the rate of reaction by blocking the active sites [205]. Pd(110), the face with lowest catalytic activity at high pressure conditions, is the most open surface and leads to the highest decomposition rate of both acetylene and benzene, showing a low percentage of bare Pd atoms [205].

The mechanism for acetylene cyclotrimerization on metal surfaces under high pressure is not unequivocally established. A

possible reaction scheme involves the concerted cyclization of three acetylene molecules [210]. Another reaction path includes the formation of a surface C_4H_4 species as a key intermediate [209,211,212]. This is followed by the insertion of another acetylene to form either an "open" C_6H_6 species and then benzene or benzene through a Diels-Alder-type addition [211,212].

XII. WATER-GAS SHIFT REACTION

The water-gas shift reaction ($CO + H_2O \rightarrow H_2 + CO_2$) is widely used industrially in various hydrogen production or enrichment processes [10,213]. Many materials are able to catalyze this reaction [10,213]. Originally, the most commonly employed industrial catalysts were based on iron oxides and operated at high temperatures (570-820K) [10,213]. A substantial improvement came about by the development of Cu/ZnO-based catalysts, which operate at relatively low temperatures (470-530K) and allow higher thermodynamic conversions [10,213]. In these catalysts, copper is the active species, and the principal role of the zinc oxide is to act as a support for the copper [10,214-218]. It is not clear why ZnO is a superior support [213-218]. In this section we review the results of studies in which the kinetics and mechanism of the water-gas shift reaction have been investigated using the modern techniques of surface science and copper single crystals.

XII.1 Kinetics on Cu(110) and Cu(111) Catalysts.

Figure 86 illustrates the effect of temperatures on the rate of the water-gas shift reaction over Cu(110) [215] and Cu(111) [214] surfaces. For the same geometric area, Cu(110) is 2.5-7.0 times more active than Cu(111) between 550 and 650K [215]. On a "per copper surface atom" basis, this difference is 1.63 larger due to the higher surface atom density of Cu(111). The slopes in Fig. 86 give apparent activation energies of 41.9 and 71.2 kJ/mol for the water-gas shift reaction on Cu(110) and Cu(111). These results indicate that the reaction is structure sensitive on copper surfaces. A fact that is consistent with data for high-surface area supported catalysts, which show an increase in the catalytic activity as the Cu particle size decreases [218]. High area supported and unsupported catalysts show apparent activation energies in the range of 54 to 67 kJ/mol [87], well within the range between Cu(110) and Cu(111) (42-71 kJ/mol).

A study of the influence of CO and H_2O partial pressures on the reaction rate over Cu(110) [215] and Cu(111) [214], revealed that on both surfaces the rate is nearly independent of P_{CO} (order $\approx$ 0) and strongly positive order in H_2O (0.5-1.0). Analysis of the surface of the catalysts with AES and XPS after reaction conditions showed essentially oxygen-free copper surfaces [214,215]. To further prove that Cu surfaces are fully reduced under water-gas shift conditions at low conversion, experiments were carried out using a heavily preoxidized Cu(111) crystal [214]. After a few minutes reaction time, the surface

111

displayed a fully metallic Cu(2p) XPS spectrum, and gave no oxygen signal in AES or XPS [87]. This suggests that metallic Cu is the active ingredient for high-surface area Cu/ZnO or Cu-based catalysts [214].

Experimental evidence supports the following mechanism for the water-gas shift reaction on Cu(110) and Cu(111) [215]:

$$H_2O_g = H_2O_a \tag{47}$$

$$H_2O_a \rightarrow OH_a + H_a \tag{48}$$

$$OH_a = O_a + H_a \tag{49}$$

$$2H_a = H_{2,g} \tag{50}$$

$$CO_g = CO_a \tag{51}$$

$$CO_a + O_a = CO_{2,g} \tag{52}$$

In this mechanism the rate-determining step involves O-H bond cleavage in H_2O_a (reaction (48)). The enhanced catalytic activity of Cu(110) compared to Cu(111) has been attributed [215] to a lower barrier for O-H bond cleavage on the Cu(110) surface. Reaction (49) may not necessarily be an elementary step, but a consequence of the process [215]:

$$H_2O_g = H_2O_a \tag{47}$$

$$H_2O_a \rightarrow OH_a + H_a \tag{48}$$

$$2OH_a = O_a + H_2O_a \tag{53}$$

$$H_2O_a = H_2O_g \tag{47}$$

$$\text{net} \quad \overline{OH_a = O_a + H_a} \tag{49}$$
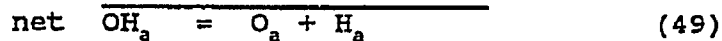
Reaction (53) provides an easy pathway for converting OH_a to O_a, which proceeds rapidly even at 290K on Cu(110) [219,220].

Figure 87 shows a potential energy diagram for the water-gas shift reaction on Cu(110). The diagram was constructed [215] using kinetic and thermochemical data for reactions (47) to (52). The activation energy for the rate determining step ($H_2O_a \rightarrow OH_a + H_a$) is ~84 kJ/mol. A value of 113 kJ/mol has been estimated for this step on Cu(111) [214]. This difference is probably due to the fact that the (110) plane is much more open, offering Cu surface atoms which are much more coordinatively unsaturated and hence more active for breaking O-H bonds.

XII.2 Sulfur Poisoning of Cu(111) Catalysts.

The poisoning of Cu/ZnO catalysts by sulfur is one of the most serious problems in the water-gas shift process [213,221]. Figure 88 shows the effect of pre-adsorbed sulfur atoms upon the rate of the water-gas shift reaction over Cu(111) [221]. Sulfur addition causes a linear decrease in the rate of the reaction, with the rate going to zero at saturation sulfur coverage ($\theta_S = 0.39$). The decay in the rate with θ_S can be easily understood in terms of a simple site-blocking model, where sulfur adatoms sterically prevent the dissociation of water [221]. The rate decay of Fig. 88 is well fit by the expression: $(1-2.6\theta_S)$. According to a statistical analysis [221], this linear function indicates that each sulfur atom blocks about 2.6 Cu atoms, and that the ensemble required for H_2O dissociation is rather small

(1 or 2 Cu atoms). This is not unexpected, given the small size of the H_2O molecule and its dissociation products (OH_a + H_a).

XII.3 Cesium Promotion of Cu(111) and Cu(110) Catalysts.

Cesium has been shown to promote the water-gas shift reaction over Cu/ZnO catalysts [222,223]. Kinetic data for the reaction on Cs promoted Cu(110) surfaces [215] are displayed in Fig. 89. The optimum Cs coverage to promote the reaction is θ_{Cs} = 0.25 ML. At this coverage, the reaction rate is five times faster than the clean surface rate at any reaction temperature [215]. The coverage dependence and optimal coverage for cesium promotion shown in Fig. 89 for Cu(110) are similar to those observed over Cu(111) [224].

An apparent activation energy of 46 kJ/mol was determined for the water-gas shift reaction on an optimally-promoted Cs/Cu(110) surface (θ_{Cs} = 0.27) [215]. This activation energy is very close to the value of 41.9 kJ/mol found for the clean surface. A tendency toward a slightly higher apparent activation energy was also observed in experiments with Cu(111), where the optimally-promoted Cs covered surface had an activation energy of 83.7 kJ/mol versus 71.2 kJ/mol for the clean Cu(111) surface [224].

A study of the pressure dependence of the water-gas shift reaction over optimally-promoted Cs/Cu(110), showed that on this surface the reaction orders in P_{CO} and P_{H2O} were very different from those on clean Cu(110) [215]. This fact rules out the

possibility that the same elementary step is rate determining with Cs present or absent.

In order to understand the role of Cs promoters in the water-gas shift reaction, detailed studies were carried out investigating the effects of Cs upon the surface chemistry of H_2O, CO and CO_2 on Cu(110) [220,225,226]. Post-reaction surface analysis of the Cs-promoted Cu(110) catalysts show that the dominant form of Cs is a surface cesium-carbonate complex (Cs•CO$_3$) [227]. This same species can be produced by dosing CO_2 to Cs/Cu(110) under ultra-high vacuum (UHV) conditions [225]. It decomposes in UHV at 450-600K (for $\theta_{Cs} < 0.25$) via: Cs•CO$_{3,a}$ → Cs•O$_a$ + CO$_{2,g}$ [225]. The equilibrium:

$$CO_{2,g} + Cs•O_a \rightleftharpoons Cs•CO_{3,a} \qquad (54)$$

occurs rapidly under water-gas shift reaction conditions [226,227]. The Cs•O$_a$ species is readily reducible with CO gas via: CO$_g$ + Cs•O$_a$ → CO$_{2,g}$ + Cs$_a$ [215,227]. Thus, a mechanism involving the species Cs•O$_a$ (produced by the reaction of H_2O and Cs [220,226,227]) rather than simply O$_a$ may be operative on the Cs promoted catalysts. The species Cs•O$_a$ should be thought as a cesium-stabilized oxygen adatom, with a dominant bond to Cu and some degree of bonding to a neighboring Cs adatom [220,226].

XIII. METHANOL SYNTHESIS

Methanol is synthesized from carbon monoxide and hydrogen by the reaction: CO + 2H_2 → CH_3OH. The selective synthesis of methanol is a process of major industrial importance because of

115

the use of methanol as a chemical intermediate, its potential use as a starting material for fuel production, and many other applications [10,228,229]. The most commonly employed industrial catalysts are based on Cu supported on ZnO, or a mixture of ZnO and other oxides such as Cr_2O_3 [10,228,229]. It has been demonstrated that under certain conditions Pd is also an active methanol synthesis catalyst, and that the nature of the support has great influence on both the rate and selectivity [230]. Here we review studies that deal with methanol synthesis on Pd(110), Cu(111), Cu(100), ZnO_x/Cu(111) and Cu/ZnO(000$\bar{1}$) single crystals.

XIII.1 Kinetics on Pd(110).

Figure 90a illustrates the effect of temperature on the rate of methanol production over a Pd(110) catalyst. The rate shows approximately Arrhenius behavior with an apparent activation energy of 77 ± 8 kJ/mol and a pre-exponential factor of $8 \times 10^4 s^{-1}$ over the temperature range of 493 to 553K [231]. The activation energy is in good agreement with values reported for Pd on "noninterating" supports such as SiO_2 and basic supports such as ZnO and La_2O_3 [231,233,234]. In addition, the pre-exponential factor determined for Pd(110) agrees well with reported values for Pd/SiO_2 [231,234]. The activation energy for Pd(110) is, however, significantly different from values obtained on acidic Al_2O_3 and TiO_2 supports [231,233].

Figure 90b shows the variation of the reaction rate with pressure at 553K. Methanol production was roughly first order

(1.2 ± 0.2) in total pressure. The specific rates seen on
Pd(110), extrapolated to pressures typical of most methanol
synthesis works, are in good agreement with rates observed for Pd
dispersed on SiO$_2$ [231,233,234]. Thus, Pd metal is an active
methanol synthesis catalyst, and no specific support interaction
is required. Highly interacting supports exhibit rates and/or
selectivities substantially different from those of Pd(110)
[231]. The rates on Pd(110) are higher than those seen over Pd
supported on zeolite and acidic supports (e.g., PdNaY and Al$_2$O$_3$)
[231,233,235], but much lower than those observed on highly
active La$_3$O$_3$-supported Pd [231,233,234].

After reaction on Pd(110), submonolayer quantities of a
carbonaceous residue (generally between 0.05 to 0.25 carbon
monolayers) were detected by Auger electron spectroscopy on the
surface of the catalyst [231]. Significant adsorption of
hydrogen into the bulk, determined by post-reaction temperature
programmed desorption, was not observed [231].

XIII.2 Studies on Cu(111), Cu(100), ZnO$_X$/Cu(111) and
Cu/ZnO(000$\bar{1}$) Surfaces.

The synthesis of methanol from CO and H$_2$ was attempted on
Cu(111) and over model catalysts consisting of well-defined Cu
overlayers on ZnO(0001) [232]. For temperatures between 500 and
600K, H$_2$ + CO total pressures up to 1500 Torr,and reaction times
of 40 minutes, no production of methanol was observed. The same
result was obtained when ZnO$_X$ films on Cu(111) were used as

catalysts [232]. On the basis of these data, an upper limit of $<2 \times 10^{-3}$ CH_3OH molecules/site-s was obtained for the catalytic activity of Cu(111), ZnO_x/Cu(111) and Cu/ZnO(000$\bar{1}$) surfaces [232]. This limit is consistent with the rates expected for high-surface area Cu/ZnO catalysts (extrapolated from a somewhat higher pressure regime) [232].

The synthesis of methanol on Cu(100) was studied in a temperature range of 500-550K at pressures between 300 and 760 Torr using a gas mixture of CO_2/CO/H_2 = 1/2/12 [236]. At 550K the reaction was first order in total pressure. Turnover frequencies for methanol production as a function of reaction temperature are shown in Fig. 91 [236]. The apparent activation energy determined from the slope of the Arrhenius plot was 73.4 kJ/mol [236]. This E_a is within the range of values (40-110 kJ/mol) reported in the literature for methanol synthesis over supported Cu catalysts.

In Fig. 91 the catalytic activity of Cu(100) is approximately one order of magnitude lower than that of silica supported Cu catalysts. It appears that Cu-oxide support interactions play an important role in creating active $Cu^{\delta+}$ sites for methanol synthesis [236]. The extremely low TCF's seen on Cu(100) are probably a consequence of the very low level of ionic copper species present in the surface under reaction conditions. Post-reaction Auger spectra showed a very small amount of oxygen on the Cu(100) surface [236].

XIV. CONCLUSIONS

The combination of a high pressure reactor with an ultra-high vacuum surface analytical chamber in the study of catalytic reactions can provide information about the molecular events that control the mechanism of reactions at the gas-solid interface. Using these techniques, the concepts of structure sensitivity and structure insensitivity can be investigated. For structure-sensitive reactions, the activity of a particular site or set of sites can be examined in detail, exploring the effects of atomic structure and electronic properties on the catalytic behavior of a surface. For structure-insensitive reactions (CO methanation, CO oxidation, etc.) excellent agreement has been obtained between studies on single crystal surfaces and studies on high surface area supported catalysts, demonstrating the relevance of kinetics measured on well-ordered single crystal surfaces for modeling the behavior of practical catalysts.

Single crystal surfaces offer an unique possibility to investigate the roles of "ensemble" and "ligand" effects on the performance of bimetallic catalysts. The works discussed above show that in some cases well-defined bimetallic surfaces (generated by vapor-depositing one metal onto a crystal face of a dissimilar metal) can have catalytic properties that are very different from those displayed by either monometallic component alone. Model studies on single crystal surfaces are also helpful in developing a better understanding of the effects of surface additives (alkali metals in ammonia synthesis, CO methanation,

water-gas shift, ethylene epoxidation, methanol synthesis, etc.)
and poisons (sulfur in CO methanation, alkane hydrogenolysis,
ethylene hydrogenation, water-gas shift, etc.) on the catalytic
activity and selectivity of metals. The influence of additives
and poisons on the surface chemistry of adsorbed reactants,
products and intermediates can be studied using UHV techniques,
and this information can be related to the effects of the
impurities upon the catalytic behavior of the metal surface. Of
particular interest is the possibility that these types of
studies will help to clarify the relative importance of
electronic and geometric contributions in determining additive
and poisoning effects.

The types of studies reviewed here, in conjunction with
accurate studies on high-surface area supported catalysts, hold
great promise for contributing to an overall understanding of
surface catalyzed reactions.

ACKNOWLEDGEMENTS